Lithostratigraphy and chemostratigraphy of salt diapir sedimentary inclusions: unraveling Ediacaran salt tectonics in the Flinders Ranges, South Australia

Kernen, Rachelle A.[1*]
rachellekernen@gmail.com
(920) 740-5687

Lehrmann, Asmara, A.[2]
alehrmanm@crimson.ua.edu
(210) 289-7824

Poe, Piper, L.[3]
piperlpoe@gmail.com
(608) 228-4069

[1]500 West University Drive, The University of Texas at El Paso
El Paso, Texas 79968

[2]One Trinity Place, Trinity University
San Antonio, TX 78212, USA

[3]Pioneer Natural Resources
777 Hidden Ridge, Irving, TX 75038, USA

[*]Corresponding Author

ABSTRACT

Patawarta Diapir, located in the Central Flinders Ranges, South Australia, has been interpreted as a single allochthonous salt sheet containing Tonian-aged igneous and layered evaporite sedimentary intrasalt inclusions derived from the Callanna Group. Using detailed field mapping, petrographic analysis, and lithostratigraphic correlation within Patawarta Diapir, five primarily silty limestone inclusions are re-interpreted as Ediacaran-aged Wonoka Formation and Patsy Hill member of the Bonney Sandstone (Wilpena Group). The Ediacaran-aged inclusions are concentrated on the diapir's south side where they are juxtaposed against 300-million-year older Tonian-aged Curdimurka Subgroup (Callanna Group) inclusion. The Ediacaran-aged silty carbonate inclusions in the Patawarta Diapir are interpreted to represent a suprasalt condensed section forming a carapace composed of Wonoka Formation and lower beds of the Patsy Hill member (Bonney Sandstone). Based on this geometric configuration, the Patawarta Diapir is composed of two separate evaporite bodies that encase the suprasalt carapace at an allosuture zone. The encasement process was likely driven by a combination of factors including regional shortening during the Delamerian Orogeny, high sedimentation rates forming local depocenters, and down-dip gravity sliding on the low-angle regional shelf. By using modern concepts in salt tectonics, this study represents the first documented example of a diagenetically altered Ediacaran Shuram Excursion due to the stratigraphy being encased in a diapir in the Flinders Ranges, South Australia.

INTRODUCTION

The Neoproterozoic Era was a pivotal interval of Earth history and the Ediacaran sedimentary succession of South Australia contains an unparalleled sedimentary record that includes complex early metazoan fossils, the Ediacaran fauna (Gehling & Droser, 2012; Plummer, 1980). The fauna was first discovered in the Ediacara Hills (Nilpena Station, northeast Finders Ranges), after which the Ediacaran Period gets its name (Preiss, 1983; Reid & Preiss, 1999). This world-famous stratigraphic succession, however, was also impacted by major salt tectonism throughout much of the Neoproterozoic and Cambrian time periods (Dalgarno & Johnson, 1968; Lemon, 1988, Rowan et al., 2019; Rowan & Vendeville, 2006). Understanding the nature and timing of salt tectonism is critical to interpret stratigraphic relationships and to make palaeoceanographic interpretations.

Salt tectonics involve long-term, ongoing syntectonic and sedimentation within affected sedimentary basins and this halokinesis is a critical factor in petroleum systems development in the Gulf of Mexico, Brazil, West Africa, and the North Sea (Diegel et al., 1995; Mohriak et al., 1995; Marton et al., 2000, Stewart and Clark, 1999). As salt nears the surface, dissolution by groundwater and seawater can occur, and a “cap” of diagenetically precipitated limestone, dolostone, or gypsum (or anhydrite) can form (Halbouty, 1979; Kyle & Posey, 1991; Poe et al., 2018; Kernen et al., 2019). This “cap” rock and any overlying sedimentary rock carapace can collapse into the diapir when underlying salt is removed due to dissolution (Halbouty, 1979; Kyle & Posey, 1991). With continued halokinesis, these rock inliers are incorporated into the evaporite sequence only to be re-exposed as the salt continues its upward movement and dissolution (Giles et al., 2012; Kernen et al., 2019). This produces complex stratigraphic relationships and is difficult to image using seismic reflection data in the subsurface (Helgesen et al., 2013; Huang et al., 2012; Li et al., 2011; Peles et al., 2004; Roy & Chazalnoel, 2011). Because syntectonic sedimentary facies change dramatically and are often eroded in proximity to the topography created by salt diapirs, biostratigraphic information is difficult to interpret proximal to a diapir. Additionally, seismic imaging within and around salt bodies can be challenging, other stratigraphic tools are needed to determine the relative and absolute age of stratigraphic sections proximal to a diapir.

We present a detailed petrographic, lithostratigraphic, and chemostratigraphic analysis of anomalous sedimentary inclusions. Inclusions are rock or sediment ranging in size from centimeters to kilometers that are, at present, contained within a salt body or diapir and are composed of any lithology different to the main diapiric strata. Patawarta Diapir, one of the major diapirs that disrupted the Ediacaran stratigraphic succession in the Flinders Ranges, South Australia, contains several large-scale, distinctive inclusions (Fig. 1). Understanding the origin and age of the inclusions is required to interpret the salt tectonic history of the diapir and to understand how this affected the adjacent sedimentary basins. This methodology is applicable to determine the stratigraphic correlation of sediment inclusions in other diapirs where conventional biostratigraphic correlation is not possible (due to age, erosion, re-working). In addition, unravelling complex stratigraphic relationships within diapirs will aid in developing paleoenvironmental, lithostratigraphic, petroleum system, and potential drilling hazards.

GEOLOGIC SETTING

The Adelaide Rift Basin (ARB) of South Australia developed through a series of continental rifting events as western Laurentia and Australia separated during the breakup of the Neoproterozoic Rodinia supercontinent (Fig. 1; Sprigg, 1952; Dyson, 1996; Preiss, 2000). The ARB is a failed rift that trends north-south extending almost 800km northward from Adelaide, South Australia through the Flinders Ranges where it bifurcates to the north into the Willouran and Gammon Ranges. The ARB contains rift-fill sediments that were deposited contemporaneously with long-lived (>250 ma), widespread, passive salt diapirism (Forbes & Preiss, 1987; Dyson, 1996; Rowan & Vendeville, 2006). After rifting ceased in the Late Neoproterozoic to early Cambrian, a major episode of crustal shortening and metamorphism followed, known as the Delamerian Orogeny, which resulted in the inversion of the failed rift system during the Late Neoproterozoic to Ordovician (~500 Ma). Shortening and inversion of the failed rift system created the Adelaide Rift Complex (Fig. 1; Forbes & Preiss, 1987; Preiss, 2000).

The Adelaide Rift Complex (ARC) contains a thick succession of strata (up to 24,000 m thick) that provides one of the most complete sedimentary records of Upper Proterozoic through Lower Cambrian depositional systems in South Australia (Preiss, 1987). The Willouran to Torrensian-aged Callanna Group at the base of the rift sequence, above Archean and Proterozoic igneous and metamorphic basement (Fig. 2), is approximately 130-8400 m thick. The Callanna Group contains the layered evaporite sequence (LES) that is composed of evaporites (halite and gypsum in the subsurface), halite-cast bearing siliciclastics, carbonates (mostly dolomite), igneous, and metamorphic rocks (Fig. 2; Forbes & Preiss 1987; Dyson, 1996; Preiss, 2000). The Callanna Group was deposited in a highly restricted marginal marine sabkha environment during the early stages of rifting (Fig. 2; Preiss, 1987). The Callanna Group is overlain by the Torrensian to Sturtian-aged Burra Group that is 3000-8000 m thick and composed of shale, siltstone, heavy-mineral laminated sandstones, and dolomites that represents the opening of the rift into a shallow ocean (Fig. 2; Preiss, 1987). The Burra Group facies reflect the transition from restricted shallow marginal lagoons to an open marine shelf (Fig. 2; Preiss, 2000). The Burra Group is overlain by Sturtian to Marinoan-aged Umberatana Group that is 6-10000 m thick and composed of diamictite, conglomerate, sandstone, and laminated siltstone (Fig. 2; Preiss, 2000). The Umberatana Group was deposited in glacial, glaciomarine, interglacial, and post-glacial marine shelf settings (Fig. 2; Preiss, 2000). The Umberatana Group is overlain by the Marinoan-aged Wilpena Group that is 40-7000 m thick and composed of dolomite, limestone, calcareous sandstone, calcareous siltstone, siliceous siltstone, and shale (Fig. 2; Preiss, 1987). The Wilpena Group was deposited in an open marine, mixed siliciclastic and carbonate shelf depositional system with occasional near shore and fluvial facies that correspond to topography created by the salt diapirs (Fig. 2; Preiss, 1987).

The Adelaide Rift Complex (ARC) contains over 180 exposed diapirs (Fig. 1; Dalgarno & Johnson, 1968; Lemon, 1988). The exposed diapirs do not display halite or gypsum at the surface but rather sedimentary and igneous inclusions that are surrounded by a diagenetic dolomicrite matrix. The diagenetic dolomicrite matrix surrounds pebble to kilometer-scale inclusions of non-evaporite lithologies generally thought to be derived entirely from the Callanna Group LES that was subsequently deformed, dismembered, and carried with the evaporite during diapirism (Fig. 2; Preiss, 1987). Both inclusions and dolomicrite matrix are collectively mapped as 'diapiric breccia' (Preiss, 1987). Mobilization of the Callanna Group evaporites and initiation of passive diapirism in the ARC began as early as the Willouran (Fig. 2; Dalgarno & Johnson, 1968). Allochthonous salt forms sheet-like salt bodies emplaced at stratigraphic levels above the autochthonous source layer (Jackson & Talbot, 1991). Allochthonous salt in the ARC was first recognized by Dalgarno & Johnson (1968) and further documented during deposition of the Burra, Umberatana, Wilpena, and Hawker Groups (Fig. 2; Dyson,1998, 2004, 2005; Lemon, 1988; Hearon et al., 2010; Kernen et al., 2012; Hearon et al.,2015a; Williams, 2017; and Rowan et al., 2019).

The autochthonous salt layer is one that rests in its original depositional position by which it accumulated by evaporation (Jackson & Talbot, 1991). Autochthonous layers of the Callanna Group LES are preserved in the Willouran and Gammon Ranges (Fig. 1). The lower part of the Callanna Group called the Arkaroola Subgroup (Fig. 2), outcrops primarily in the Gammon Ranges near Mount Painter and Arkaroola. Within the Arkaroola Subgroup the Wooltana Volcanics, located in the Gammon and Flinders Ranges have been radiometrically dated to 827 +/-6 to 830 +/-50 Ma (Fig. 2; Preiss, 1987). The relatively younger part of the Callanna Group is called the Curdimurka

Subgroup, which outcrops in the Willouran Ranges (Fig. 2; Preiss, 1987). Preiss (1987) states that, in the Flinders Ranges, autochthonous exposures of the Callanna Group LES are not present. Rather, it is interpreted that the Callanna Group stratigraphic units are exclusively preserved as inclusions within the diapiric breccia (diapiric to allochthonous salt) in the Flinders Ranges. Because the inclusions are no longer in their original depositional position (autochthonous), stratigraphic correlation from the Flinders Ranges diapiric Callanna Group to the autochthonous Callanna Group LES in the Willouran and Gammon Ranges is problematic (Fig. 1; Preiss, 1987). Due to our inability to correlate the Callanna Group stratigraphy from the Willouran and Gammon Ranges to the Flinders Ranges, different names have been given to stratigraphic units are thought to be relatively the same age (Fig. 3; Preiss, 1987).

Within the autochthonous Callanna Group stratigraphy, few carbonate units have been documented (Fig. 2). The Dunns Mine Limestone has been documented in the Willouran Ranges and the slightly younger Waraco Limestone in the Flinders Ranges (Preiss, 1987). The Dunns Mine Limestone varies between 50-200m thick and is composed of dark gray dolostone interbedded with beds of calcareous shale and siltstone and lenses of sandstone (Murrell, 1977). Additionally, chalcedonic nodules are found in the dolomite of the lower part of the section (Murrell, 1977). The Waraco Limestone is composed of pale gray to cream stromatolitic dolostone and calcitic to dolomitic marble (Preiss, 1987). The paucity of limestone in the Callanna Group stratigraphy is significant because this contrasts to large silty limestone inclusions that are common in the Patawarta Diapir identified in this study.

Previous Work Patawarta Diapir

Kernen et al., (2012) documented the detailed sedimentology and mapped the stratigraphy adjacent to the southern margin of Patawarta Diapir and Gannaway (2014) documented the detailed sedimentology and mapped the stratigraphy adjacent to the northern margin of the Patawarta Diapir (Figs. 4 & 5). A summary of the sedimentology from the detailed work of Kernen et al. (2012) and Gannaway (2014) is recorded and summarized in Tables 1-2 (Figs. 4 & 5). The following units adjacent to Patawarta Diapir that directly pertain to this study are: (1) lower limestone member of the Wonoka Formation (Nwwll); (2) middle limestone member of the Wonoka Formation (Nwwlm); (3) upper limestone member of the Wonoka Formation (Nwwlu); (4) green mudstone member of the Wonoka Formation (Nwwgm); and (5) lower dolomite beds of the Patsy Hill member (Npbpdl). Based on the previous work of Haines (1988), Kernen et al., (2012) and Gannaway, (2014), the stratigraphy surrounding Patawarta Diapir has been interpreted to be deposited in a shallowing upward wave-dominated shelfal setting (Lower Wonoka-Green Siltstone members of the Wonoka Formation) to a tidally dominated tidal inlet setting (Patsy Hill members of the Wonoka Formation).

The Patawarta Diapir is roughly $4km^2$ and is interpreted as an allochthonous salt body or a sheet-like salt body emplaced at stratigraphic levels above the autochthonous (LES) source layer (Jackson & Talbot, 1991; Rowan & Vendeville, 2006; Kernen et al., 2012; Hearon et al., 2015a; Rowan et al., 2019). Patawarta Diapir itself contains abundant inclusions of sedimentary units up to several kilometers wide (Appendix Figs. 1 & 2) that were roughly mapped by Hall (1984) and interpreted as being from the autochthonous Tonian-aged Callanna Group LES. The inclusions contain the following lithologies: heavy mineral laminated sandstone and quartzite containing ripple cross-lamination and halite pseudomorphs, thin interbeds of heavy mineral laminated sandstone and thinly bedded, green-brown calcareous siltstone and shale, thinly bedded green-brown and gray calcareous and dolomitic shale and siltstone containing halite casts, thinly bedded black limestone with finely bedded calcareous shale and siltstone, weakly brecciated dolomite, red shale, amygdaloidal basalt and fine-grained dolerite (Appendix Figs. 1& 2; Hall, 1984). The thinly bedded black-green limestone and calcareous siltstones and shales are not lithologies documented in the relatively age-equivalent autochthonous Callanna LES in the Willouran and Gammon Ranges, however, they are common inclusion lithologies in the southern part of the Patawarta Diapir and are the focal point for this study (Appendix Figs. 1 & 2).

Kernen et al. (2012) interpreted the sedimentary strata along the southern margin of Patawarta Diapir as a subsalt minibasin (Fig. 6; small basins, or depressions, that fill with sediment located *below* an allochthonous salt sheet; Jackson & Hudec, 2017). Gannaway (2014) originally described and interpreted the sedimentary strata along the northern margin of Patawarta Diapir as a suprasalt minibasin (Fig. 6; small basins, or depressions, that fill with sediment *above* an allochthonous salt sheet). The subsalt and suprasalt minibasins contains Wilpena Group strata of the upper Bunyeroo Formation, Wonoka Formation (lower, middle, upper members & green siltstone member), Patsy

Hill Member of the Bonney Sandstone (lower and upper dolomite beds, lower and upper sandstone beds), and the lower Bonney Sandstone (Tables 1-2; Figs. 4 & 5; Kernen et al., 2012; Gannaway, 2014). All stratigraphic units thin, onlap, and dip away from the diapir recording the halokinetic sequence history of the of the diapir (Kernen, 2011; Giles & Lawton, 2002; Giles & Rowan, 2012; Kernen et al., 2012; Gannaway, 2014). Based on the stratigraphic geometry of the subsalt minibasin, the upper Bunyeroo Formation, Wonoka Formation, and Patsy Hill member (Bonney Sandstone) form one tapered halokinetic sequence in the subsalt minibasin adjacent to Patawarta Diapir (Fig. 6; Kernen et al., 2012). Based on the stratigraphic geometry of the suprasalt minibasin, the upper Bunyeroo Formation, Wonoka Formation, and Patsy Hill member (Bonney Sandstone) thin and onlap Patawarta Diapir while the upper-most portion of the Patsy Hill member forms a thin carapace or roof over Patawarta Diapir (Fig. 6; Kernen et al., 2012; Gannaway, 2014).

METHODS

A 1:36,000 scale geological map of the limestone inclusions in the Patawarta Diapir was created and built on previous work (Figs. 6 & 7; Kernen et al., 2012; Gannaway, 2014). Within the mapped area, five stratigraphic sections were measured in detail including lithology, grain size, fresh and weathered colors, bedding orientation and stratigraphic contacts. Approximately 200 samples were collected to document the range of lithologies and varying mineralogies of the inclusions. 100 petrographic thin sections were prepared and stained for calcite and iron with alizarin red-S and potassium ferricyanide and analyzed in both plane- and cross-polarized light; matrix, cements, and grain types and mineralogy were documented.

Fifty-eight limestone and dolostone samples were analyzed for $\delta^{13}C$ and $\delta^{18}O$ values at the University of Michigan and University of Kansas stable isotope laboratories. Samples were slabbed perpendicular to bedding and 5 to 10 mg of powder were generated by micro-drilling the diapiric matrix, rim dolomite caprock, inclusion 3, and lower, middle, and upper Wonoka formations, and Patsy Hill Member of the Bonney Sandstone from the suprasalt and subsalt minibasins. Because inclusion 3 contained all the representative carbonate inclusion lithologies, two samples were collected from Lithofacies 1 and one sample from the other lithofacies (Lithofacies 2-5). All powders were heated under vacuum in individual borosilicate reaction vials to 200°C to remove volatile contaminants and water. Carbonate samples weighing a minimum of 10 micrograms were placed in stainless steel boats. Samples were then placed in individual borosilicate reaction vessels and reacted at 76 °C with 3 drops of H_3PO_4 on a Finnigan MAT Kiel I preparation device coupled directly to the inlet of a Finnigan MAT 251 triple collector isotope ratio mass spectrometer. $\delta^{13}C$ and $\delta^{18}O$ were acquired simultaneously on both systems, and isotopic data are reported in the standard delta notation (‰) relative to the VPDB standard (Vienna Pee Dee Belemnite). Precision and accuracy are monitored by running 14 standards for every 72 unknowns. The standard set included a primary standard (NBS-19) and a secondary, in-house marble standard. All samples were measured relative to an internal gas standard, and then converted to the VPDB scale using the known composition of NBS-19 ($\delta^{13}C$ = 1.95‰; $\delta^{18}O$ = -2.20‰). Measured precision was 0.05 to 0.1 ‰ for $\delta^{13}C$ and 0.15 to 0.2 ‰ for $\delta^{18}O$.

Cathodoluminescence petrography (CL) was performed using a Relion ELM-3R Luminoscope in the University of Wisconsin-Oshkosh Geology Department. The voltage was held between 13 and 15 kV, with current ranging from 480 to 570 mA, and chamber vacuum between 50 and 60 millitorr. Photomicrographs in CL were used to recognize diagenetic alteration of the carbonate inclusions. Polarized-light microscopy was performed using polished, 30µm-thick thin sections, analyzed using a Nikon Eclipse E400 POL petrographic microscope to document carbonate mineralogy.

RESULTS

Intrasalt Inclusion Sedimentology

Five sedimentary inclusions containing primarily silty limestone, calcareous siltstone, and shale were identified within the southwestern part of Patawarta Diapir (Figs. 8 & 9; Tables 3 & 4). The inclusions are bounded by diapiric matrix or mafic igneous sills (Figs. 10 & 11) and are characterized by internally coherent bedding trends that define an internal stratigraphy. That internal stratigraphy is marked by five distinct lithofacies (1-5), which were mapped in detail (Figs. 8, 9, 10). Inclusion 1 is located the farthest north in the Patawarta Diapir and is 1.5 km by 0.3 km. It displays steep dips (up to 90°) that gradually decrease northward to approximately 45° (Fig. 10; Tables 4-5). Inclusion 2 is located south of inclusion 1. Inclusion 2 is 1.0 km by 0.4 km and displays a recumbent fold with steep dips (50-60°) to the west and shallow dips to the east (20-30°; Fig. 10; Tables 4-5). Inclusion 3 is located directly south of inclusion 2. Inclusion 3 is 0.8 km by 0.25 km and displays steeper dips (50-75°) to the west and shallower dips to the east (30-50°). Inclusion 4 is located south of inclusion 3 and southwest of inclusion 5. Inclusion 4 is 1.0 km by 0.20 km and displays relatively consistent NW-SE trending 40-50° dips on the northwestern side that steepen to 90° and are tightly folded on the southeastern side. Inclusion 5 is directly northeast of inclusion 4 and is the largest inclusion. Inclusion 5 is 1.1 km by 1.2 km and displays varying dips (30-60°) that form a large recumbent fold (Fig. 10; Tables 4-5). The northern, western, and southern margins of the five inclusions are in contact with the diapiric matrix and the eastern portion is covered by recent alluvium (Fig. 10).

The inclusion lithofacies are described here in ascending stratigraphic order starting with Lithofacies 1 (Tables 3 & 4). Lithofacies 1 is 22-60 m thick and is composed of gray to tan, thinly laminated (1-3 mm) calcareous siltstone and silty lime mudstone that form beds 1-5 cm thick (Figs. 8a, 9a, 10). Lithofacies 1 is dominated by calcareous siltstone at the base with decreasing quartz silt stratigraphically upward where the beds become carbonate rich. Lithofacies 1 is always in contact with the diapiric matrix at the lower boundary and is only found in inclusions 3 and 4; the upper boundary is in contact with Lithofacies 2 in both inclusions (Fig. 11; Tables 3 & 4). Lithofacies 2 is 30-55 m thick and composed of tan and gray, thinly laminated (1-5 mm) silty lime mudstone interbedded with lime mudstone that forms beds 5-10 cm thick (Figs. 8b, 9b, 10). Lithofacies 2 is dominated by silty lime mudstone at the base and decreasing quartz silt content up-section where the beds become lime mudstone.

Lithofacies 2 is only found in inclusions 3 and 4 where it is overlies Lithofacies 1 and underlies Lithofacies 3 (Fig. 11; Tables 3 & 4). Lithofacies 3 is 6-70 m thick and composed of tan, thinly laminated (5-10 mm) silty lime mudstone interbedded with lime mudstone that forms beds 10-30 cm thick (Figs. 8c, 9c, 10). It is dominated by silty lime mudstone at the base and decreases in quartz silt content up-section. Lithofacies 3 is found in inclusions 1-5 where it consistently lies stratigraphically below Lithofacies 4. Lithofacies 3 overlies Lithofacies 2 in inclusions 3 and 4 (Fig. 11; Tables 3 & 4). Lithofacies 4 is 6-200 m thick and is composed of dark greenish black to light green, thinly laminated (3-5 mm) calcareous siltstone to shale that form beds 1-5 cm thick (Figs. 8d, 9d, 10). Lithofacies 4 is dominated by calcareous siltstone at the base with apparent thin bedding while the upper portion is dominated by a massive green siltstone that is non-calcareous. Lithofacies 4 is found in inclusions 1-5 and overlies Lithofacies 3 (Fig. 11; Tables 3 & 4). Lithofacies 5 is 3-30 m thick and is composed of tan, thinly laminated (1-3 mm) sandy dolomite (calcite cement) that forms laminae 5-10 mm thick with local symmetrical wave-rippled horizons and rare massive bedding (Figs. 8e, 9e, 10). Lithofacies 5 is found in inclusions 1-3 and stratigraphically above Lithofacies 4 (Fig. 11; Tables 3 & 4).

Based on outcrop and petrographic sedimentological attributes and stratigraphic order, Lithofacies 1-5 are lithostratigraphically correlated to Wonoka and Patsy Hill member of the Bonney Sandstone stratigraphic map units in the suprasalt and subsalt minibasins. In ascending order: (1) Lithofacies 1 is equivalent to the lower limestone member of the Wonoka Formation; (2) Lithofacies 2 is equivalent to the middle limestone member of the Wonoka Formation; (3) Lithofacies 3 is equivalent to the upper limestone member of the Wonoka Formation; (4) Lithofacies 4 is equivalent to the green mudstone member of the Wonoka Formation; and (5) Lithofacies 5 is equivalent to the lower dolomite beds of the Patsy Hill member (Table 5). Because the stratigraphy lacks wave and current sedimentary structures, 'stratigraphic up' and the correlation was determined by the specific stratigraphic order of lithologies. The order of Lithofacies 1-5 matches the order of the lower-green siltstone members of the Wonoka Formation and lower dolomite beds of the Patsy Hill member (Bonney Sandstone). Based on outcrop and petrographic lithologic attributes and stratigraphic order, Lithofacies 1-5 are lithostratigraphically correlative to the Wonoka Formation and Patsy Hill Member of the Bonney Sandstone stratigraphic map units in the suprasalt and subsalt minibasins. Based on this correlation, the silty carbonate inclusions are identified as Ediacaran-age Wonoka Formation and Patsy Hill Member (Bonney Sandstone) not units of the Callanna Group as had been previously interpreted by Coats (1973) and Hall (1984).

The subsalt and suprasalt Wonoka Formation lower limestone member display horizontal laminae and reduction spots in the lime mudstone beds, hummocky cross-stratification in the silty lime mudstone, and micaceous siltstone beds suggest deposition in an outer shelf below storm wave-base that shallows to a lower shoreface depositional environment (Preiss, 1987; Haines, 1988, 1990; Walker and Plint, 1992; Kernen et al., 2012; Gannaway, 2014; Table 6). The subsalt and suprasalt Wonoka Formation middle limestone member displays hummocky cross stratification in the calcareous siltstone beds overlain by calcareous siltstone beds and low angle cross-bedding, asymmetrical and symmetrical ripples in the quartz arenite sandstones beds allow it to be interpreted as being deposited within the lower to upper shoreface depositional environment with the sandstone beds deposited in the foreshore (Haines, 1988, 1990; Walker and Plint, 1992; Kernen et al., 2012; Gannaway, 2014; Table 6). The upper limestone member of the Wonoka Formation is interpreted to be deposited in the foreshore depositional environment (Haines, 1988, 1990; Walker and Plint, 1992; Kernen et al., 2012; Gannaway, 2014: Table 6). The green mudstone member of the Wonoka Formation lacks current and wave sedimentary structures and is interpreted to be deposited in a coastal plain depositional environment (Haines, 1988; 1990; Kernen et al., 2012; Gannaway, 2014; Table 6). The Patsy Hill lower dolomite beds are interpreted to be deposited in a tidally-dominated main tidal channel inlet depositional environment (Colquhoun, 1995; Kernen et al., 2012; Gannaway, 2014; Table 6), based on the rhythmically interbedded dark gray dolomite and pyrite-rich black shale, quartzite pebble conglomerate and sand stringers that scour into the underlying algal laminite.

The sedimentary structures of the lower, middle, upper, and green siltstone member of the Wonoka Formation *inclusions* are limited (horizontal laminae almost exclusively) and therefore each member or bed is interpreted to be deposited in either a terrestrial to lagoon depositional environment. The lower dolomite beds of the Patsy Hill member display wavy bedding which likely indicates crypt-algal laminae; therefore, it is most likely that Lithofacies 5 was deposited in shallow water-lagoonal depositional environment which is nearly identical to the subsalt and suprasalt minibasins.

The lithologic order of Lithofacies 1-5 matches the lithologic order of the lower, middle, upper, and green siltstone members of the Wonoka Formation and lower dolomite beds of the Patsy Hill member (Bonney Sandstone) in the subsalt and suprasalt minibasins. All members of the Wonoka Formation and lower dolomite beds of the Patsy Hill member contain intraformational conglomerates (coarse sand-pebble sized) that are related to the uplift and halokinesis of Patawarta Diapir during the depositional history and formation of the suprasalt and subsalt minibasins. However, the inclusion stratigraphy lacks the intraformational conglomerates which indicates that halokinesis did not take place and it most likely formed as a roof or carapace (Hart et al., 2004).

Stable Isotope Results & Diagenesis

$\delta^{13}C$ and $\delta^{18}O$ isotopes from limestone and dolomite inclusions, caprock, diapir matrix, sub-and suprasalt minibasins were analyzed and plotted stratigraphically and compared to previous regional data and the adjacent minibasin stratigraphy (Fig. 12 & 13). The $\delta^{13}C$ and $\delta^{18}O$ isotope values were measured from Lithofacies 1-5 within Inclusion 3 at stratigraphic section 3 (Figs. 10, 11, 12, 13). Six samples were collected in total; two samples from Lithofacies 1 and one sample each from Lithofacies 2-5 (Figs. 10, 11, 12, 13). $\delta^{13}C$ and $\delta^{18}O$ isotopes of the six samples from Inclusion 3 were plotted (grey oval; Fig. 13). The $\delta^{13}C$ and $\delta^{18}O$ isotope values from Inclusion 3 plots within the range of values for the Shuram Excursion in the adjacent minibasin succession, however the other five values are more positive than expected (Figs. 12, 13, 14).

In order to understand the isotopic variation of the inclusions, thin sections were examined under cathodoluminescence (CL; Fig. 15). The geochemical data from inclusion stratigraphic section 3 (type section) of the Wonoka Formation and Patsy Hill Member are presented in a stratigraphic framework to compare to the inclusion lithofacies and to assess the effects of diagenesis. Lithofacies 1 is comprised of a lime mudstone with fine-grained crystalline matrix that luminesces brown-orange with calcite-rich veins that luminesces orange-yellow in CL and crosscuts Lithofacies 1 (Fig. 15a & 15b). Lithofacies 3 is comprised of a silty limestone matrix that luminesces orange-dark orange and is crosscut by orange-yellow-luminescing calcite veins and quartz cement replacing gypsum (Fig. 15c & 15d). Lithofacies 5 is dominated by a silty dolomite matrix that is dark brown/black under CL which is crosscut by calcite veins that luminesce orange-yellow under CL (Fig. 15e & 15f).

DISCUSSION

Evolution of the Diapir

The inclusions in map view currently appear as individual 'mega-clasts' in the diapir surrounded by diapiric matrix which may indicate that it was once a large panel of stratigraphy that was subsequently faulted and folded by post-halokinesis movement and encasement. Once a carapace is encased and incorporated into a diapir, it is defined as suture (Dooley et al., 2012). Dooley et al. (2012) describes two types of sutures, one type referred to as an autosuture which is a panel of stratigraphy that separates two lobes from a single salt sheet and the other type referred to as allosuture which is a panel of stratigraphy that separates two coalesced salt sheets. There are two types of allosutures, one being a frontal allosuture whereby its map trace is roughly perpendicular to the main direction of salt flow and a lateral allosuture whereby a suture whose map trace is roughly parallel to the main direction of salt flow (Dooley et al., 2012). We are not able to distinguish between a lateral or frontal allosuture in this study because of the two-dimensional nature of outcrop studies.

The Ediacaran-aged inclusions in Patawarta diapir are forming an allosuture based on a combination of the following observations: the distribution of the layered evaporite sequence Tonian-aged Curdimurka Subgroup inclusions are concentrated to the northern side of the diapir and the significantly younger Ediacaran-aged Wonoka Formation and Patsy Hill member inclusions are concentrated to the southern side of the diapir (Fig. 16 & 17). An equal distribution of inclusions throughout Patawarta Diapir would suggest all the inclusions are relatively the same age. Our second line of evidence to support an allosuture interpretation is the detailed stratigraphic changes from the suprasalt minibasin (Giles et al., 2017) and subsalt minibasin (Lehrmann et al., 2017) suggest the suprasalt minibasin was not depositionally connected to the subsalt minibasin. Because the detailed stratigraphy of the Wonoka Formation and lower dolomite beds of the Patsy Hill Member from the suprasalt and subsalt minibasins are slightly different in terms of water depth and thickness compared to the stratigraphy of the inclusions, the carapace is interpreted to represent either a lateral or frontal allosuture (Table 5 & 6). The sedimentary structures within the suprasalt and subsalt minibasins capture the overall shallowing upward sequence of the third order highstand systems tract that is not seen in the inclusion stratigraphy (Tables 5 & 6; Kernen et al., 2012). If the detailed stratigraphy of the Wonoka Formation and Patsy Hill Member were identical in the suprasalt and subsalt minibasins and inclusions, an autosuture (Dooley et al., 2012) would be a more likely interpretation. Our third line of evidence to support an allosuture interpretation is that one salt sheet is thought to be sourced from the northwest, with internal flow represented by the LES Tonian-aged Curdimurka Subgroup sheath fold (Fig. 17; Rowan et al., 2019), and the other sheet was likely sourced from the southeast based on the orientation of the halokinetic fold in the subsalt Bunyeroo Formation established by (Fig. 17; Hearon et al., 2015a). If the sheath fold and halokinetic fold were orientated in the same direction, an autosuture interpretation would be more plausible.

The frontal or lateral allosuture at Patawarta Diapir could have been encased by the following salt tectonic processes: 1) one salt sheet overriding another salt sheet, 2) one salt sheet overriding a flared diapir, or 3) the amalgamation of two or more diapirs or salt sheets. It is conceivable that the encasement of the carapace was initiated by a combination of the following processes: 1) the Delamerian Orogeny (Preiss, 2000), 2) low-angle gravity sliding that takes place on the shelf, and 3) high sedimentation rates in the suprasalt minibasin. Based on the regional map geometry of the connecting salt bodies (diapiric breccias), it is likely that a salt body was sourced from the northern side of Patawarta Diapir and the thickened Wonoka Formation suprasalt depocenter provided the sedimentary loading mechanism for a salt body on the northern side of the diapir to override a salt body on the southern side of the diapir, thus encasing the carapace in the diapiric matrix and forming an allosuture (Fig. 16 & 17). With the interpretation of an allosuture, Patawarta Diapir is reinterpreted to represent at least two diapirs instead of a single diapir as originally mapped by Coats (1973) and Hall (1984; Figure 17).

Chemostratigraphy & Diagenesis

Previous studies on the Shuram Excursion in the Flinders Ranges, South Australia provides a variety of explanations for its origin such as 1) primary dissolved inorganic carbon (DIC), 2) meteoric diagenesis, 3) burial diagenesis, or 4) authigenic carbonate (Husson et al., 2015). The first model for the origin of the Shuram Excursion is when carbon isotope compositions of unaltered carbonates ($\delta^{13}C$ carb) precipitated in equilibrium with seawater reflects the composition of dissolved inorganic carbon (DIC) reservoir in the oceans, as precipitation of carbonates involves little isotopic fractionation relative to the DIC pool (Hayes & Waldbauer, 2006; Halverson et al., 2010; Schmid, 2017). Carbon isotopes constrain primary productivity and organic matter burial where the organisms prefer to uptake light carbon isotopes ^{12}C against ^{13}C during chemical reactions. Therefore, organic material will be enriched in light carbon isotope compared to the original pool of carbon. The second model for the origin of the Shuram Excursion in South Australia is through meteoric diagenesis (Husson et al., 2015). Meteoric diagenesis is interpreted as a result of recrystallization in the presence of CO_2 rich fluids, derived from organic matter in soils (Knauth and Kennedy, 2009; Swart and Kennedy, 2012). Sourced from δ18O depleted rainwater, these fluids can create covarying δ13C carb and δ18O carb ranges as they mix with marine waters heavier in both δ13C carb and δ18O carb (Allan and Matthews, 1982). The third model for the origin of the Shuram Excursion in South Australia is through burial diagenesis where an extreme depletion in δ13C carb was acquired significantly after burial of the Ediacaran sediments (ie. under 2–3 km of overburden, at 100 °C; Derry, 2010). Shuram-like excursion profiles result from alteration by a mixture between a high *p*CO2, low δ13C carb fluid, developed from respired buried organic matter, and an δ18O rich basinal brine (Derry, 2010). The fourth model for the origin of the Shuram Excursion in South Australia is the development of authigenic carbonate in very δ13C depleted carbonate environment during early sediment diagenesis (Schrag et al., 2013).

Abrupt changes in the $\delta^{13}C$ ratios are known as carbon isotope excursion events that are used as a correlation tool to a known basin wide event. Those excursion events are typically given a name and are compared to excursions and sequence stratigraphy in other sedimentary basins. The oldest documented Neoproterozoic carbon isotope excursion in the Tonian (Willouran and Torrensian) is called the 'Bitter Springs' excursion which is located in the Amadeus Basin Bitter Springs Formation (Limestone) near Alice Springs (Fig. 14; Klaebe, 2015). The Bitter Springs excursion is approximately δ^{13} C -3‰ to -4‰ PDB (Pee Dee Belemnite) and the stratigraphic equivalent formation in the Willouran or Flinders Ranges is not clear as a proper correlation and is yet to be discovered and described (Stueken et al., 2019). The second oldest carbon isotope excursion is called the 'Islay' excursion which contains the most negative carbon isotopic signature at δ^{13} C -9‰ however, there is an unconformity during this time in the Willouran and Flinders Ranges and strata of that age are not found (Fig. 14; Condon et al., 2015). The ‘Keele Peak’ in the Marinoan Umberatana Group is the only positive carbon isotope excursion at δ^{13} C +12‰ (Fig. 14; Condon et al., 2015). The ‘Trezona’ excursion in the Marinoan Umberatana Group becomes the most negative at δ^{13} C -7‰ and is documented in the Flinders Ranges stratigraphy (Fig. 14; Condon et al., 2015). The youngest Marinoan excursion is referred to as the Ediacaran-aged Shuram excursion (Fike et al., 2006; Grotzinger, et al., 2011; Husson et al., 2015; Le Guerroué et al., 2010), which has δ^{13} C values as low as -12‰, thus constituting the most negative δ^{13} C excursion known in Earth’s history (Fig. 14; Husson et al., 2015). In this study, the Shuram Excursion is documented in the Wonoka Formation adjacent to Patawarta Diapir, however the inclusions of Wonoka Formation stratigraphy inside the Patawarta Diapir have been diagenetically altered, therefore altering the Shuram Excusion isotope signature.

When comparing the δ^{13}C results to the regional Wonoka Formation and Patsy Hill member data from Husson et al. (2015), Lithofacies 1-3 have higher values, Lithofacies 4 has a similar value, and Lithofacies 5 has slightly lower values (Figs. 12 & 13). The δ^{13}C values of the diapiric matrix and rim dolomite are higher relative to those of the regional Wonoka Formation (Husson et al., 2015) and to the results from the Wonoka Formation in this study (Figs. 13 & 14). An interpretation of the isotopically positive results from the diapiric matrix and rim dolomite are yet to be published and require further detailed analysis and interpretation. The δ^{18}O values from the lower Wonoka Limestone member are similar to the published regional δ^{18}O values (Husson et al., 2015), however, there is no obvious correlation with the other members of the carbonate inclusion stratigraphy.

The results of the $\delta^{13}C$ geochemistry, along with the outcrop and petrographic observations with cathodoluminescence (CL) microscopy, suggest that the inclusions are diagenetically altered limestones of the Wonoka Formation and Patsy Hill member. The $\delta^{13}C$ results from the inclusions are not as negative as reported by Husson et al.'s, (2015) regional study of -12‰. The -12‰ value is not captured in our results for following two reasons: 1) lowermost part of Lithofacies 1 could be missing due to an erosional unconformity or it was never deposited or 2) the $\delta^{13}C$ results are diagenetically altered from fluid flow within Patawarta diapir (Fig. 15). The positive $\delta^{13}C$ values of the diapiric matrix and rim dolomite also indicates that a post-encasement fluid flow event took place, partially replacing the original $\delta^{13}C$ values which resulted in a positive $\delta^{13}C$ signature. The $\delta^{18}O$ isotope results are not consistent with Husson et al., (2015) which supports the hypothesis that post-encasement fluid flow took place (Figs. 13, 14, 15). CL microscopy of Lithofacies 3 and 5 indicate a calcite-rich diagenetic event took place after the encasement of the inclusions, thus being the source of the diagenetic alteration of rocks deposited during the Shuram Excursion (Fig. 15).

CONCLUSION

Patawarta Diapir contains inclusions that are ca. 300 million years younger than previously thought. The Wonoka Formation and Patsy Hill Member (Bonney Sandstone) inclusions suggest active halokinesis during the Ediacaran era. The sedimentology and stratigraphic relationships of inclusions 1-5 in the Patawarta Diapir are described in detail and correlated to the Wonoka Formation and Patsy Hill Member (Bonney Sandstone) in the adjacent suprasalt and subsalt minibasins. The presence of isopachous inclusion stratigraphy allow for the inclusions to be interpreted as a carapace, a condensed section deposited above a diapiric body. Additionally, the Wonoka Formation and Patsy Hill Member (Bonney Sandstone) inclusions are stratigraphically thinner than the equivalent strata in the subsalt or suprasalt minibasins which supports the carapace interpretation. Because the disrupted remnants of carapace are now surrounded by diapiric matrix in Patawarta Diapir, it is interpreted that the carapace was encased by one salt diapir overriding another forming an allosuture. The mechanisms for encasement are poorly constrained, however, they could be possible through regional shortening of the Delamerian Orogeny, high sedimentation rates in the suprasalt minibasin, and low angle gliding along the regional shelf. The Callanna Group sheath fold indicates the diapir was flowing to the northeast and is separated by the disrupted allosuture while the halokinetic fold in the subsalt Bunyeroo Formation indicates that southern portion of the diapir was flowing toward the south. The difference in salt flow direction supports the interpretation that the Wonoka Formation and Patsy Hill member inclusions form an allosuture. The results of the $\delta^{13}C$ and $\delta^{18}O$ stable isotope geochemistry suggest that the Wonoka Formation and Patsy Hill member inclusions contain a diagenetically altered Shuram Excursion within the Patawarta Diapir. The stable isotope geochemical data are supplemented by cathodoluminescence microscopy and indicate a calcite-rich diagenetic fluid flow event took place post-encasement of the Wonoka Formation and Patsy Hill member inclusions and thus altered their $\delta^{13}C$ and $\delta^{18}O$ signatures. These data conclude that fluid flow takes place in diapirs, especially when they contain inclusions or heterogenous lithologies.

ACKNOWLEDGEMENTS

The field research and geochemical analyses were funded by present and past corporate sponsors of the Salt–Sediment Interaction Research Consortium, first at New Mexico State University (as the Institute of Tectonic Studies) and later at The University of Texas at El Paso (Anadarko, BHP, BP, Chevron, ConocoPhillips, Devon, ExxonMobil, Hess, Kosmos, Marathon, Nexen, Repsol, Samson, Shell, Statoil (Equinor), Total), the American Association of Petroleum Geologists Grants-In-Aid, the Society of Professional Earth Scientists Award, the University of Texas El Paso Geological Sciences Bruce Davidson Memorial Award, the West Texas Geological Society Award, the Roswell Geological Society Award, the University of Texas El Paso Geological Sciences Hunt and Rowling Scholarship and the Vernon G. and Joy Hunt Endowed Scholarship.

REFERENCES

Allan, J. R., and Matthews, R. K., 1982, Isotope signatures associated with early meteoric diagenesis: Sedimentology, v. 29, n. 6, p. 797–817, http://dx.doi.org/10.1111/j.1365-3091.1982.tb00085.

Coats, R.P., 1973, COPLEY map sheet and explanatory notes, Geological Atlas of South Australia 1:250,000 series, Geological Survey of South Australia.

Colquhoun, G.P, 1995, Siliciclastic sedimentation on a storm- and tide-influenced shelf and shoreline, Early Devonain Roxburgh Formation, northeastern Lachlan Fold Belt, southeastern Australia. Sedimentary Geology, v. 97, p. 63-93.

Condon, D., Zhu, M., Bowring, S., Wang, W., Yang,A., Jin, A., 2005, U–Pb ages from the Neoproterozoic Doushantuo Formation, China, Science, 308, p. 95-98.

Dalgarno, C. R., & Johnson, J. E., 1968, Diapiric structures and Late Precambrian–Early Cambrian sedimentation in Flinders Ranges, South Australia. In J. Braunstein & G. D. O'Brien (Eds.), AAPG Memoir. Diapirs and diapirism p. 301–314. Tulsa, OK: American Association of Petroleum Geologists.

Derry, L. A., 2010, A burial diagenesis origin for the Ediacaran Shuram-Wonoka carbon isotope anomaly: Earth and Planetary Science Letters, v. 294, n. 1–2, p. 152–162, http://dx.doi.org/10.1016/j.epsl.2010.03.022.

Diegel, F. A., J. F. Karlo, D. C. Schuster, R. C. Shoup, andP. R. Tauvers, 1995, Cenozoic structural evolution andtectonostratigraphic framework of the northern Gulf Coastcontinental margin,inM. P. A. Jackson, D. G. Roberts,and S. Snelson, eds., Salt tectonics: A global perspective:AAPG Memoir 65, p. 109–151.

Dooley, T. P., Hudec, M. R., Jackson, M. P. A., 2012, The structure and evolution of sutures in allochthonous salt, AAPG Bulletin, v. 96, No. 6, p. 1045–1070.

Dyson, I. A., 1998, The 'Christmas tree diapir' and salt glacier at Pinda Springs, central Flinders Ranges. MESA Journal, 10, p. 40–43.

Dyson, I. A., 2004, Geology of the eastern Willouran Ranges – evidence for earliest onset of salt tectonics in the Adelaide Geosyncline. MESA Journal, 35, p. 48–56.

Dyson, I. A., 2005, Evolution of allochthonous salt systems during development of a divergent margin: The Adelaide Geosyncline of South Australia. In P. P. Post, N. C. Rosen, D. L. Olson, S. L. Palmes, K. T. Lyons, & G. B. Newton (Eds.), Proceedings of the 25th Annual Bob F. Perkins Research Conference. Petroleum systems of divergent continental margin basins p. 69–89. Houston, TX: Gulf Coast Section, SEPM.

Fike, D. A., Grotzinger, J. P., Pratt, L. M., Summons, R. E., 2006, Oxidation of the Ediacaran ocean, Nature, 444, p. 744-747.

Forbes, B. G., & Preiss, W. V., 1987, Stratigraphy of the Wilpena Group. In W. V. Preiss (Ed.), The Adelaide Geosyncline – Later Proterozoic stratigraphy, sedimentation, paleontology, and tectonics. Geological Society of Australia Bulletin Vol. 53, p. 211–248. Adelaide, SA: Department of Mines and Energy, Geological Survey of South Australia.

Gannaway, C. E., Giles, K.A., Kernen, R.A., Rowan, M.G., Hearon, T.E., IV, 2014, Comparison of Suprasalt and Subsalt Depositional and Halokinetic History of Patawarta Diapir, Flinders Ranges, South Australia: American Association of Petroleum Geologists 2014 Annual Conventions Abstracts Volumes, Houston, TX.

Gehling, J.G., Droser, M.L., 2012, Ediacaran stratigraphy and the biota of the Adelaide Geosyncline, South Australia, Episodes, 35/1, pp236-246.

Giles, K. A., & Lawton, T. F., 2002, Halokinetic sequence stratigraphy adjacent to the El Papalote diapir, northeastern Mexico. AAPG Bulletin, 86, p. 823–840.

Giles, K. A., and Rowan, M. G., 2012, Concepts in halokinetic–sequence deformation and stratigraphy, in G. I. Alsop, S. G. Archer, A. J. Hartley, N. T. Grant, and R. Hodgkinson, eds., Salt Tectonics, Sediments and Prospectivity, Geological Society of London Special Publications, v. 363, p. 7-31, doi: 10.1144/SP363.2.

Giles, S., Kernen, R.A., Lehrmann, A., Giles, K., 2017, Evolution of a suprasalt minibasin: Neoproterozoic (Ediacaran) Patawarta salt sheet, Flinders Ranges, South Australia, Geological Society of America South Central Annual Conventions Abstracts Volumes, San Antonio, TX.

Grotzinger, J. P., Fike, D. A.,Fischer, W. W., 2011, Enigmatic origin of the largest-known carbon isotope excursion in Earth's history, Nature Geoscience, 4, p. 285-292.

Hall, D., 1984, The mineralization and geology of Patawarta Diapir, northern Flinders Ranges, South Australia, Honours thesis, University of Adelaide, (unpublished).

Haines, P. W., 1988, Storm-dominated mixed carbonate/siliciclastic shelf sequence stratigraphy displaying cycles of hummocky cross-stratification, late Proterozoic Wonoka Formation, South Australia. Sedimentary Geology, 58(2–4), p. 237–254. doi:10.1016/0037-0738(88)90071-1.

Haines, P. W., 1990, A late Proterozoic storm-dominated carbonate shelf sequence: The Wonoka Formation in the central and southern Flinders Ranges, South Australia. In J. B. Jago & P. S. Moore (Eds.), The evolution of a Late Precambrian–Early Paleozoic rift complex: Adelaide geosyncline p. 117–198. Sydney, NSW: Geological Society of Australia, Special Publication v. 16.

Halbouty, M. T., 1979, Salt domes—Gulf region, United States and Mexico, 2nd edition: Houston, Texas, Gulf Publishing, p. 561.

Halverson, G., Wade, B., Hurtgen, M., & Barovich, K., 2010, Neoproterozoic chemostratigraphy. Precambrian Research, 182(4), p. 337-350.

Hart, W., Jaminski, J., and Albertin, M., 2004, Recognition and Exploration Significance of Suprasalt Stratal Carapaces, Salt-Sediment Interactions and Hydrocarbon Prospectivity: Concepts, Applications, and Case studies for the 21st century, p. 166-199.

Hayes, J., & Waldbauer, J., 2006, The carbon cycle and associated redox processes through time. Philosophical Transactions of the Royal Society of London. Series B, Biological Sciences, 361(1470), p. 931-950.

Hearon, T. E., IV, Lawton, T. F., & Hannah, P. T., 2010, Subdivision of the upper Burra Group in the eastern Willouran Ranges, South Australia. MESA Journal, 59, p. 36–46.

Hearon, T.E., IV, Rowan, M.G., Giles, K.A., Kernen, R.A., Gannaway, C.E., Lawton, T.F., Fiduk, C.J., 2015, Allochthonous salt initiation and advance in the northern Flinders and eastern Willouran ranges, South Australia: using outcrops to test subsurface-based models from the northern Gulf of Mexico, American Association of Petroleum Geologists Bulletin.

Helgesen, H. K., Tang, J., Liu, J., Salama, A., Pepper, R., Madden, S., Woodward, M., Klebleeva, A., Frugier-Dorrington, E., El Sabaa, A., Yarman, C. E., Fournier, A., Yang, Y., Osypov, K. S., 2013, Dirty Salt Velocity Model Building: Society of Exploration Geophysicists Annual Meeting, Houston, p. 5.

Huang, W., Jiao, K., Vigh, D., Kapoor, J., Watts, D., Hongyan, L., Derharoutian, D., Cheng, X., Application of full-waveform inversion for salt sediment inclusion inversion: Society of Exploration Geophysicists Annual Meeting, Las Vegas, p. 5.

Husson J. M., Maloof A. C., Schoene B., Chen C. Y. and Higgins J. A., 2015, Stratigraphic expression of Earth's deepest d13C excursion in the Wonoka Formation of South Australia. Am. J. Sci. 315, 1–45.

Jackson, M. P. A., and Talbot, C. J., 1991, A glossary of salt tectonics: The University of Texas at Austin: Bureau of Economic Geology Geological Circular, 91-4, p. 44.

Jackson, M., & Hudec, M., 2017, Minibasins. In Salt Tectonics: Principles and Practice (pp. 155-180). Cambridge: Cambridge University Press. doi:10.1017/9781139003988.010.

Kaebe, R. M., 2015, The palaeoenvironmental context of Neoproterozoic carbonisotope excursions, The University of Adelaide School of Physical Sciences (PhD Dissertation unpublished). Adelaide, South Australia.

Kernen, R. A., 2011, Halokinetic sequence stratigraphy of the Neoproterozoic Wonoka Formation at Patawarta Diapir, Central Flinders Ranges, South Australia: Master's thesis, New Mexico State University, Las Cruces, New Mexico (master's thesis unpublished).

Kernen, R.A., Giles, K.A., Lawton, T.F., Rowan, M.G., Hearon, T.E., IV, 2012, Depositional and halokinetic sequence stratigraphy of the Neoproterozoic Wilpena Group adjacent to Patawarta allochthonous salt sheet, central Flinders Ranges, South Australia in G. I. Alsop, S. G. Archer, A. J. Hartley, N. T. Grant, and R. Hodgkinson, eds., Salt Tectonics, Sedimentation and Prospectivity: London, Geological Society of London Special Publication 363, p. 81-105.

Kernen, R.A., Giles, K. A., Poe, P., Gannaway, C.E., Rowan, M.G., Fiduk, J.C., Hearon, T.E., 2019, Origin of the Rim Dolomite as Lateral Caprock, Flinders Ranges, South Australia. Australian Journal of Earth Sciences.

Knauth, L. P., and Kennedy, M. J., 2009, The late Precambrian greening of the Earth: Nature, v. 460, p. 728–732, http://dx.doi.org/10.1038/nature08213

Kyle, J. R., and Posey H. H., 1991, Halokinesis, Cap Rock Development, and Salt Dome Mineral Resources. Evaporites, Petroleum and Mineral Resources. Ed. J. L. Melvin. N.p.: Elsevier. p. 413-74.

Lehrmann, A., Kernen, R. A., Giles, S., Giles, K., 2017, Timing of allochthonous salt emplacement of the Neoproterozoic (Ediacaran) Patawarta salt sheet, Flinders Ranges, South Australia: Evidence from the subsalt minibasin, Geological Society of America South Central Annual Conventions Abstracts Volumes, San Antonio, TX.

Le Guerroué, E., 2010, Duration and synchroneity of the largest negative carbon isotope excursion on Earth: the Shuram/Wonoka anomaly Comptes Rendus Geoscience, 342 (2010), pp. 204-214.

Lemon, N. M., 1988, Diapir recognition and modelling with examples from the late proterozoic Adelaide Geosyncline, Central Flinders Ranges, South Australia. Ph.D. thesis, University of Adelaide, Department of Geology and Geophysics.

Li, Z., Ji, S., Bai, B., Wu, Q., Han, W., Dirty Salt Tomography Using RTM 3D Angle Gathers; Society of Exploration Geophysicists Annual Meeting, San Antonio, p. 5.

Marton, G., G. Tari, and C. Lehmann, 2000, Evolution of the Angolan passive margin, West Africa, with emphasis on post-salt structural styles; in Webster Mohriak and Manik Talwani, eds., Atlantic Rifts and Continental Margins: American Geophysical Union Geophysical Monograph Series 115, p. 129–149.

Mohriak, W. U., M. Nemčok, and G. Enciso, 2008, South At-lantic divergent margin evolution: Rift-border uplift andsalt tectonics in the basins of SE Brazil,inR. J. Pankhurst,R. A. J. Trurow, B. B. Briton Neves, and M. J. De Wit,eds., West Gondwana: Pre-Cenozoic correlations acrossthe South Atlantic region: Geological Society SpecialPublication 294, p. 365–398.

Murrell, B., 1977, Statigraphy and Tectonics across the Torrens Hinge Zone Between Andamooka and Marree, South Australia. Victoria University of Wellington (BSc unpublished).

Peles, O., Bartana, A., Kosloff, D., Koren, Z., 2004, Limitations of the exploding reflector model in sub-salt imaging, Society of Exploration Geophysicists Annual Meeting, Denver, p. 3.

Plummer, P.S., 1980, Circular structures in a Late Precambrian sandstone: Fossil medusoids or evidence of fluidization? Royal Society of South Australia. Transactions, 104(1), p13-16

Poe, P.L., Giles K.A., Brunner, B., Kernen, R.A., Labrado, A., Lerer, K., 2018, Classification of caprock associated with salt diapirs. Penrose conference "Advances in salt tectonics: observations, applications, and perspectives: In honor of Martin P.A. Jackson". Ein Boqeq, Dead Sea, Israel. Poster.

Preiss, W.V., 1983, Adelaide Geosyncline and Stuart Shelf, South Australia, 1:600 000 Precambrian and Palaeozoic geology map (with special reference to the Adelaidean). 1st edition., Geological Survey of South Australia, 1v, Map.

Preiss, W. V., 1987, The Adelaide Geosyncline-late Proterozoic stratigraphy, sedimentation, palaeontology and tectonics: Geological Survey of South Australia Bulletin v. 53, p. 438.

Preiss, W. V., 2000, The Adelaide Geosyncline of South Australia and its significance in Neoproterozoic continental reconstruction: Precambrian Research, v. 100, p. 21-63.

Reid, P. W., & Preiss, W. V., 1999, PARACHILNA map sheet (second ed.): Geological Atlas 1:250 000 Series, Sheet SH54-13. Adelaide SA: South Australia Geological Survey.

Rowan, M. G., & Vendeville, B. C., 2006, Foldbelts with early salt with-drawal and diapirism: Physical model and examples from the north-ern Gulf of Mexico and the Flinders Ranges, Australia. Marine and Petroleum Geology, 23(9–10), p. 871–891. doi:10.1016/j.marpetgeo. 2006.08.003.

Rowan, M. G., Hearon, T. E., Kernen, R. A., Giles, K. A., Gannaway, C. E., Williams, N. J., Hannah, P. T., 2019, A review of allochthonous salt tectonics in the Flinders and Willouran ranges, South Australia. Australian Journal of Earth Sciences, 66. doi:10.1080/08120099. 2018.1553063.

Roy, A., and Chazalnoel, 2011, RTM technology for improved salt imaging in the Santos Basin, Brazil: Society of Exploration Geophysicists Annual Meeting, San Antonio, p. 5.

Schmid, S., 2017, Neoproterozoic evaporites and their role in carbon isotope chemostratigraphy (Amadeus Basin, Australia). Precambrian Research, 290, p. 16-31.

Schrag, D. P., Higgins, J. A., Macdonald, F. A., and Johnston, D. T., 2013, Authigenic carbonate and the history of the global carbon cycle: Science, v. 339, n. 6119, p. 540–543, http://dx.doi.org/10.1126/science.1229578.

Sprigg, R. C., 1952, Sedimentation in the Adelaide Geosyncline and the formation of a continental terrace, in M. F. Glaessner and E. A. Rudd, eds., Sir Douglas Mawson Anniversary Volume: Adelaide, University of Adelaide, p.153–159.

J.A. Clark, J.A. Cartwright, S.A. Stewart, Mesozoic dissolution tectonics on the West Central shelf, UK Central North Sea, Marine and Petroleum Geology, Volume 16, Issue 3, 1999, Pages 283-300, ISSN 0264-8172, https://doi.org/10.1016/S0264-8172(98)00040-3.

Stüeken, E., E., Buick, R., Lyons, T., W., 2019, Revisiting the depositional environment of the Neoproterozoic Callanna Group, South Australia, Precambrian Research, Volume 334, 105474, ISSN 0301-9268, https://doi.org/10.1016/j.precamres.2019.105474.

Walker, R.G. and Plint, A.G., 1992, Wave- and Storm-Dominated Shallow Marine Systems, In: Facies Models Response to Sea Level Change, Memorial University of Newfoundland St. John's, Newfoundland and Labrador, Geological Association of Canada, p. 219-238.

Williams, N. J., 2017, Structural evolution and paleohydrology of a tertiary salt weld, Willouran Ranges, South Australia (Unpublished master's thesis). Northern Illinois University, DeKalb, IL.

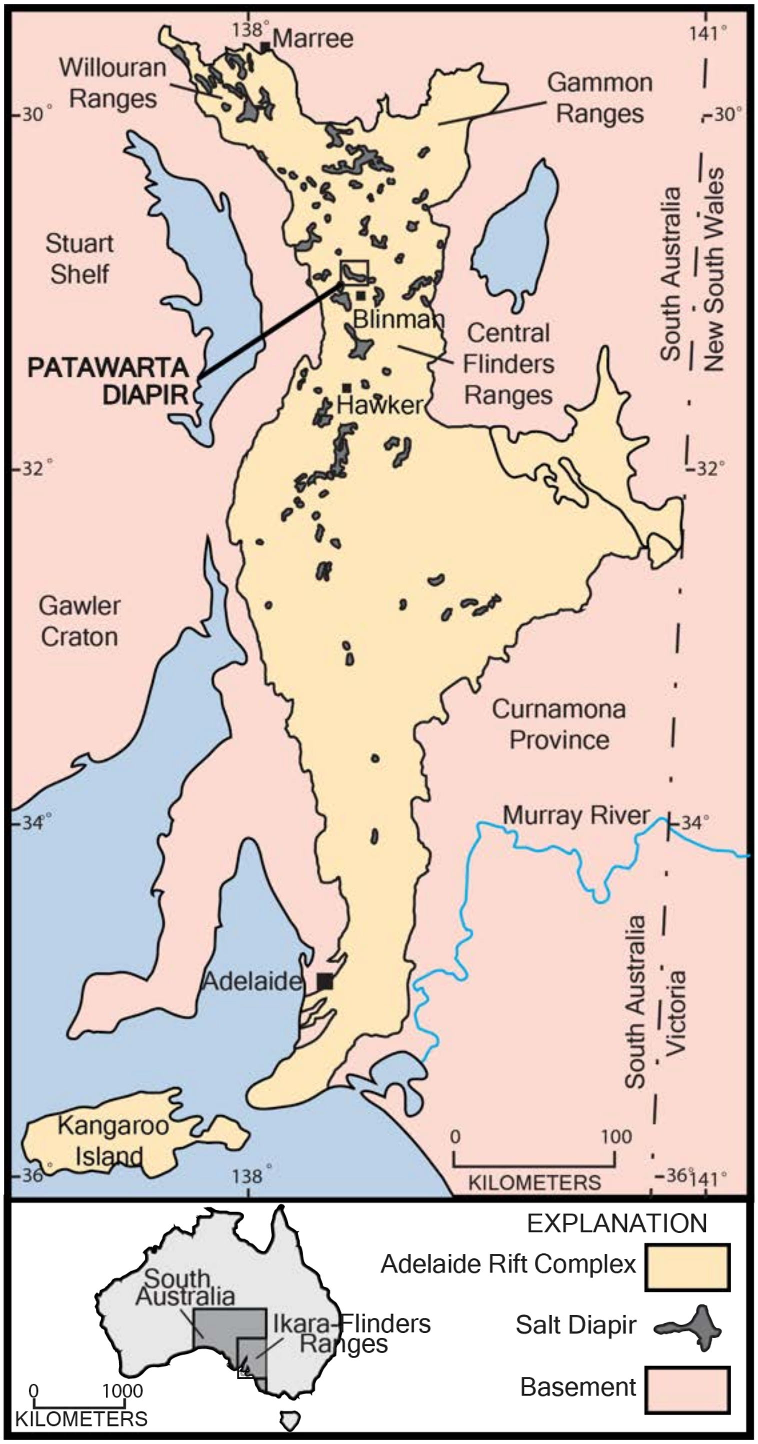

Figure 1-Map of the Adelaide Rift Complex (ARC) of South Australia displaying the location of major diapirs, including the Patawarta Diapir in the Central Flinders Ranges (modified from Kernen et al., 2012; after Dalgarno & Johnson, 1968).

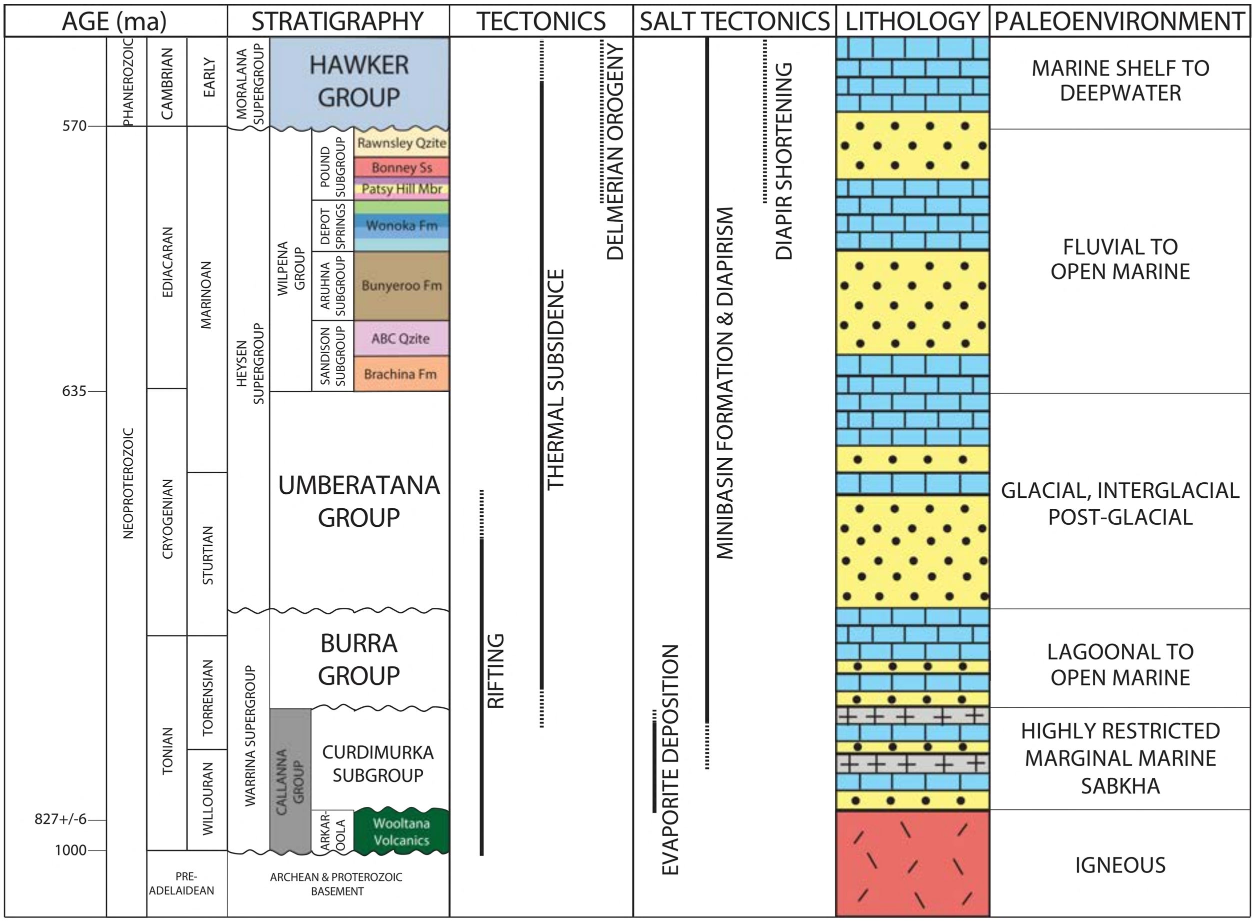

Figure 2-Precambrian–Cambrian stratigraphy, regional tectonics, salt tectonics, lithology, and paleoenvironments of the Adelaide Rift Complex in the Central Flinders Ranges, South Australia (modified from Preiss, 1987). The colors under 'Stratigraphy' correspond to the map units in Fig. 6. Under 'Lithology,' blue corresponds to carbonate, yellow corresponds to siliciclastic, grey corresponds to evaporites, and red corresponds to igneous.

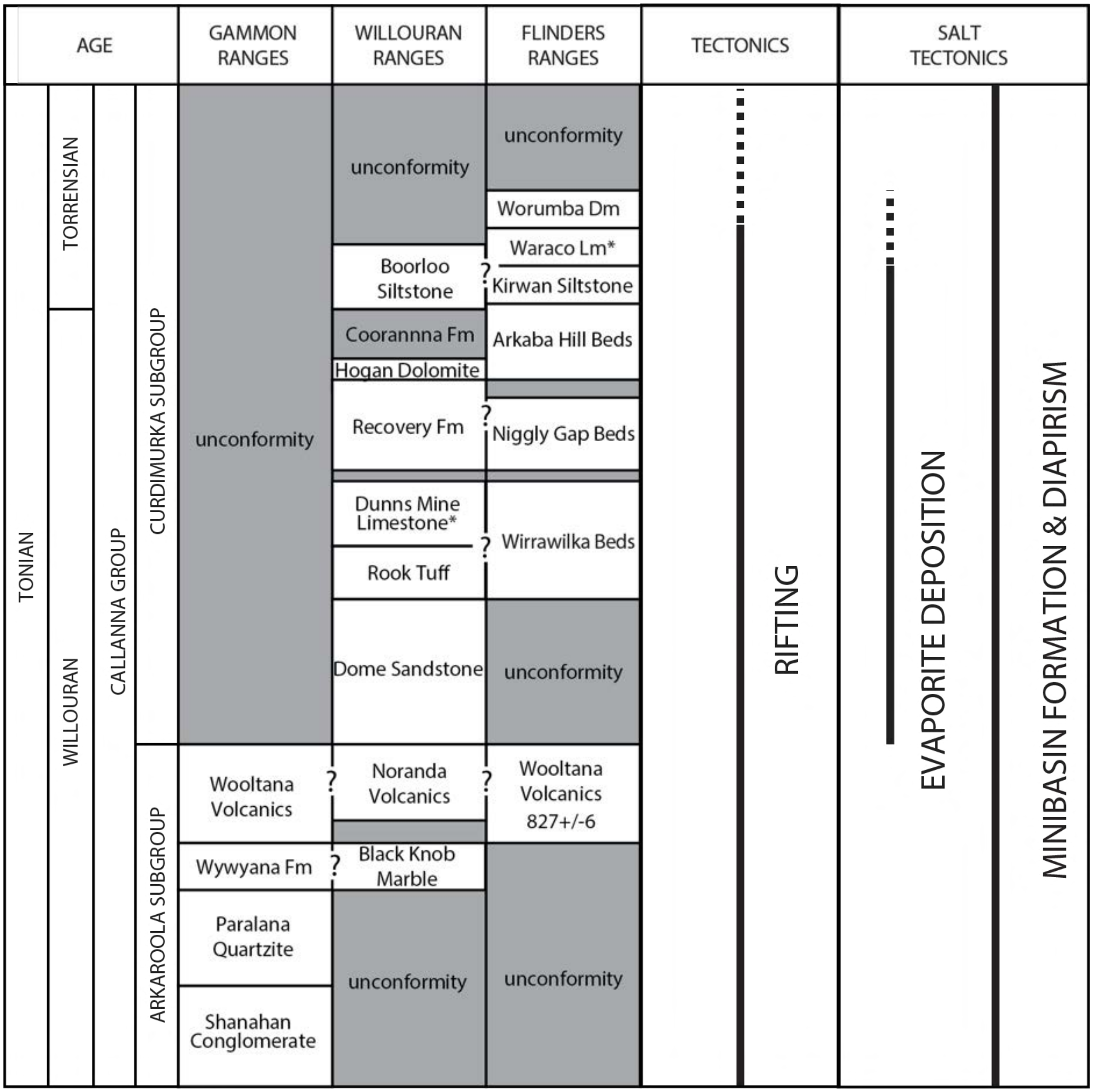

Figure 3-Stratigraphy, tectonics, and salt tectonics of the Tonian-aged Callanna Group layered evaporite sequence in the Gammon, Willouran, and Flinders Ranges (modified from Preiss, 1987). The Callanna Group strata in the Gammon and Willouran Ranges are located in their original layered evaporite sequence. The Callanna Group strata in the Flinders Ranges are located in the diapirs as inclusions.

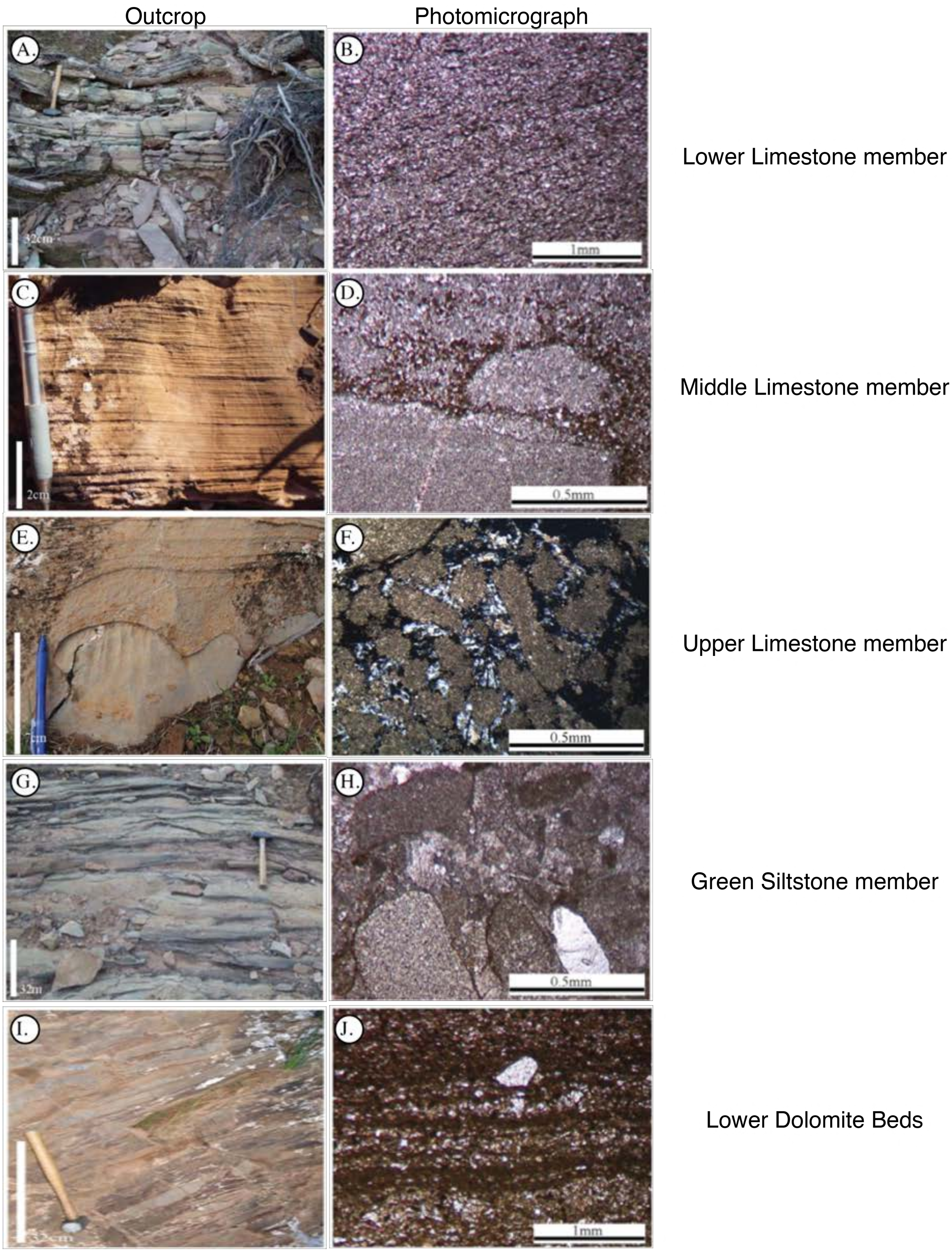

Figure 4-A) Outcrop photograph and B) photomicrograph in polarized light of the lower limestone member, C) outcrop photograph and D) photomicrograph in polarized light of

the middle limestone member, E) outcrop photograph and F) photomicrograph in polarized light of the upper limestone member, and G) outcrop photograph and H) photomicrograph in plane light of the green siltstone member (Wonoka Formation; collected from subsalt stratigraphic section R) and I) outcrop photograph and J) photomicrograph in polarized light of the lower dolomite beds (Patsy Hill member; collected from subsalt stratigraphic section U; from Kernen, 2011).

SUMMARY OF SUBSALT SEDIMENTOLOGY					
Lithofacies	Lithology	Color	Bedding	Grain Size	Sedimentary Structures
lower dolomite	dolomite, shale, sandstone	dark gray, black	4-6 cm	silt, medium sandstone	horizontal to wavy laminae-bedding, diapiric detritus
green siltstone	lime mudstone, silty limestone	green, yellow	1mm-1cm	silt	horizontal laminae-bedding, diapiric detritus
upper limetsone	silty limestone, calcareous sandstone	blue gray, purple	30 cm-2 m	silt, medium sandstone	horizontal laminae-bedding, soft-sediment deformation, stylonondular texture, low angle crossbeds
middle limestone	silty limestone, calcareous sandstone	blue gray, red	1 mm-30 cm	silt, medium sandstone	horizontal laminae-bedding, flute casts, HCS, low angle crossbeds, asymmetrical & symmetrical ripples, rip-up clasts
lower limestone	lime mudstone, silty limestone	red, purple, light green	1 mm-20 cm	silt, medium sandstone	horizontal laminae-bedding, flute casts, HCS, low angle crossbeds, asymmetrical & symmetrical ripples, rip-up clasts, diapiric detritus

Table 1-Summary of subsalt sedimentological characteristics (data summarized from Kernen 2011).

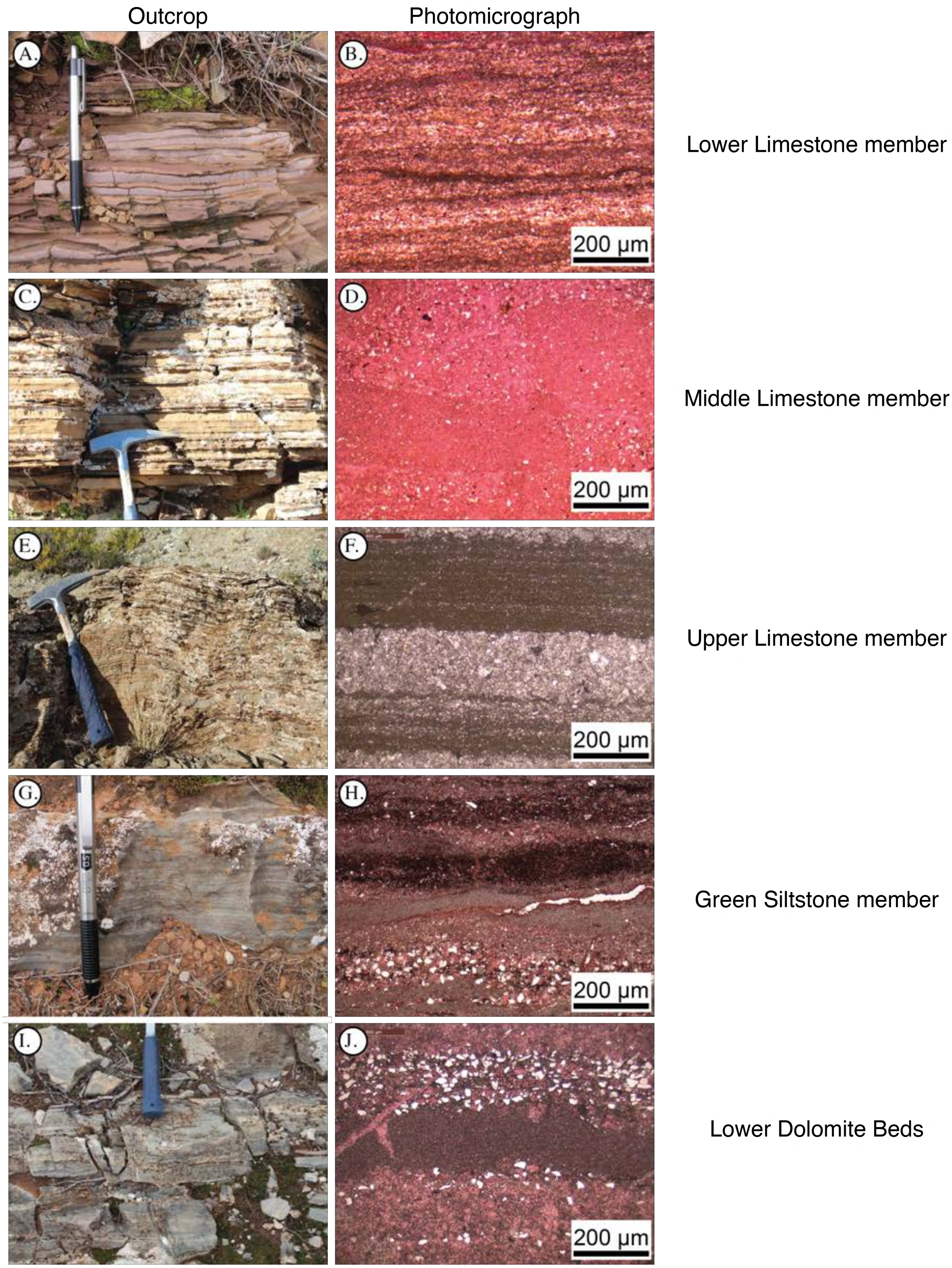

Figure 5-A) Outcrop photograph and B) photomicrograph in polarized light of the lower limestone member, C) outcrop photograph and D) photomicrograph in plane light of the

middle limestone member, E) outcrop photograph and F) photomicrograph in plane light of the upper limestone member, and G) outcrop photograph and H) photomicrograph in polarized light of the greensiltstone member (Wonoka Formation; collected from suprasalt stratigraphic section B) and I) outcrop photograph and J) photomicrograph in plane light of the lower dolomite beds (Patsy Hill member; collected from suprasalt stratigraphic section C; from Gannaway, 2014).

SUMMARY OF SUPRASALT SEDIMENTOLOGY					
Lithofacies	Lithology	Color	Bedding	Grain Size	Sedimentary Structures
lower dolomite	dolomite, calcareous sandstone	dark gray, tan	2 cm-1 m	silt, medium sandstone	horizontal to wavy laminae-bedding, diapiric detritus, karst
green siltstone	lime mudstone, silty limestone	green, yellow	1 mm-8 cm	silt	horizontal laminae-bedding, low angle crossbeds, symmetrical ripples, diapiric detritus
upper limetsone	lime mudstone, silty limestone	blue gray, red, purple	2 mm-1 m	silt	horizontal laminae-bedding, soft-sediment deformation, stylonondular texture, symmetrical ripples, rip-up clasts
middle limestone	silty limestone, calcareous sandstone	blue, gray, red	3 mm-1.5 m	silt, medium sandstone	horizontal laminae-bedding, flute casts, HCS, low angle crossbeds, asymmetrical & symmetrical ripples, rip-up clasts
lower limestone	lime mudstone, silty limestone	red, purple, green-gray	3 mm-40 cm	silt, medium sandstone	horizontal laminae-bedding, flute casts, HCS, low angle crossbeds, asymmetrical & symmetrical ripples, rip-up clasts, diapiric detritus

Table 2-Summary of suprasalt lithologic characteristics (data summarized from Gannaway, 2014).

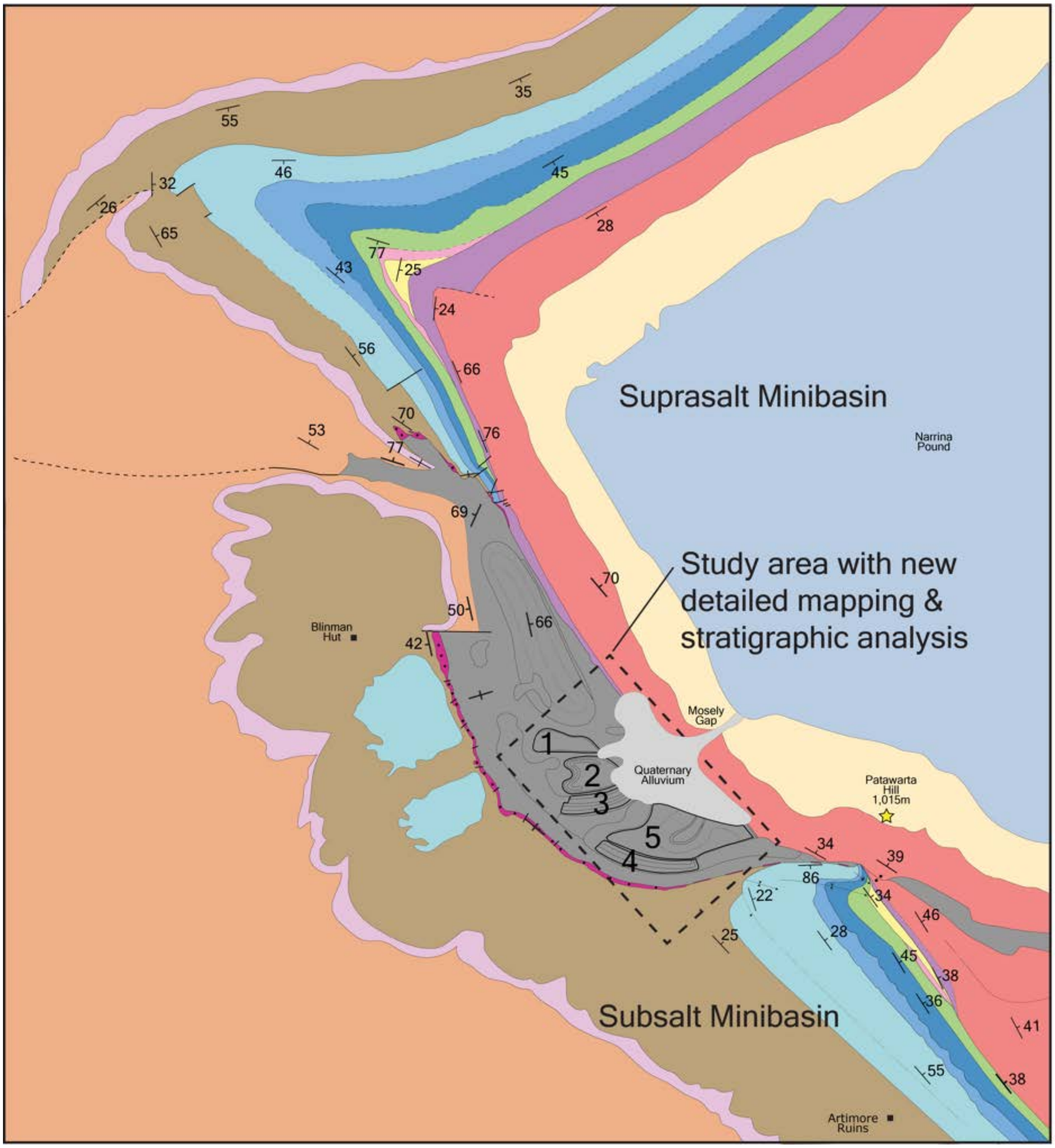
Suprasalt Minibasin
Narrina Pound
Study area with new detailed mapping & stratigraphic analysis
Blinman Hut
Mosely Gap
Quaternary Alluvium
Patawarta Hill 1,015m
Subsalt Minibasin
Artimore Ruins

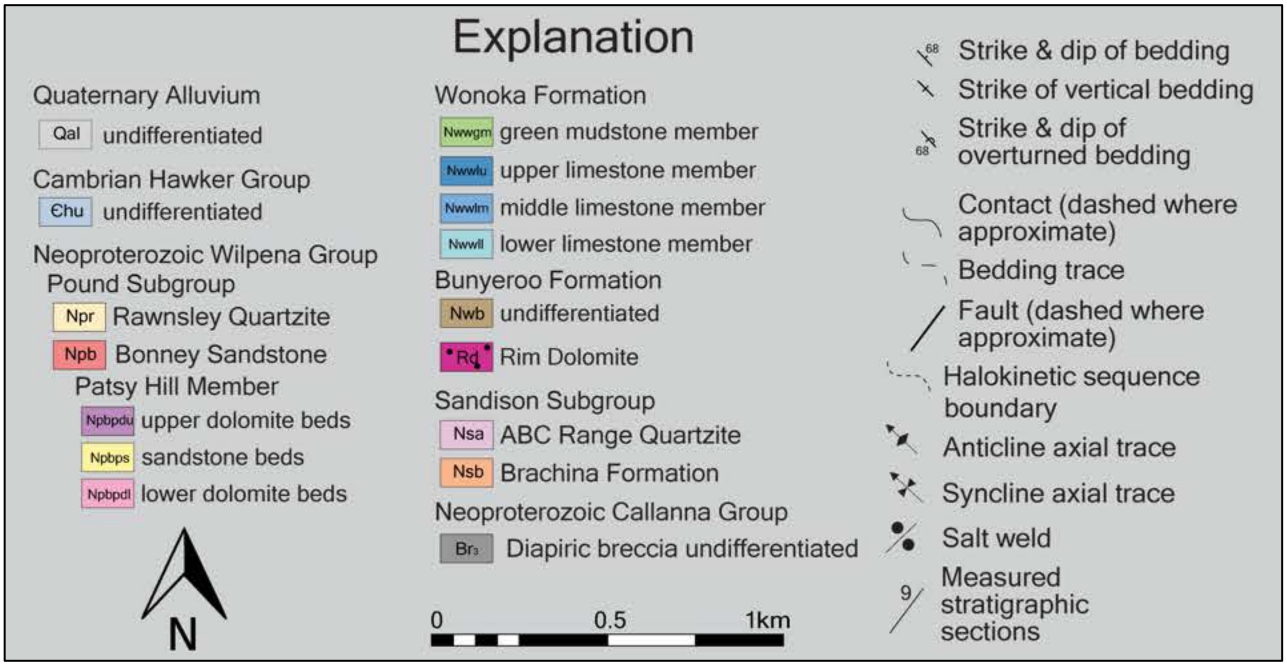

Figure 6-Geologic map of Patawarta Diapir in the Flinders Ranges, South Australia (modified from Gannaway, 2014; Kernen et al., 2012). Study area located in the dashed box where numbers 1-5 depict inclusions—see Fig. 10.

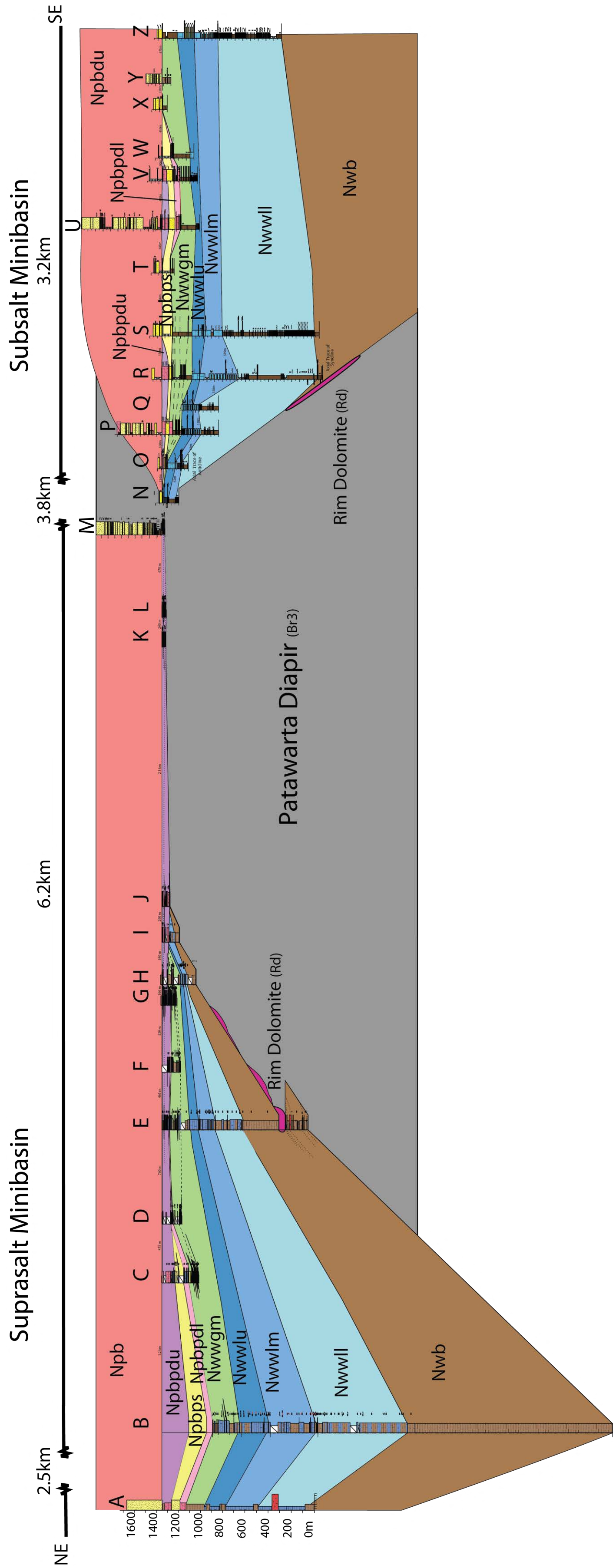
NE
SE
2.5km
6.2km
3.8km
3.2km
Suprasalt Minibasin
Subsalt Minibasin
Patawarta Diapir (Br3)
Rim Dolomite (Rd)
Rim Dolomite (Rd)
A
B
C
D
E
F
G
H
I
J
K
L
M
N
O
P
Q
R
S
T
U
V
W
X
Y
Z
Npb
Npbpdu
Npbps
Npbpdl
Nwwgm
Nwwlu
Nwwlm
Nwwll
Nwb
Npbdu
Npbpdl
Npbpdu
Npbps
Nwwgm
Nwwlu
Nwwlm
Nwwll
Nwb
1600
1400
1200
1000
800
600
400
200
0m

Figure 7-Correlation diagram of the sedimentology and thickness changes in the suprasalt and subsalt minibasins (combined from Gannaway, 2014; Kernen et al., 2012) Colors and symbols for formations and members are same as those shown in Fig. 6.

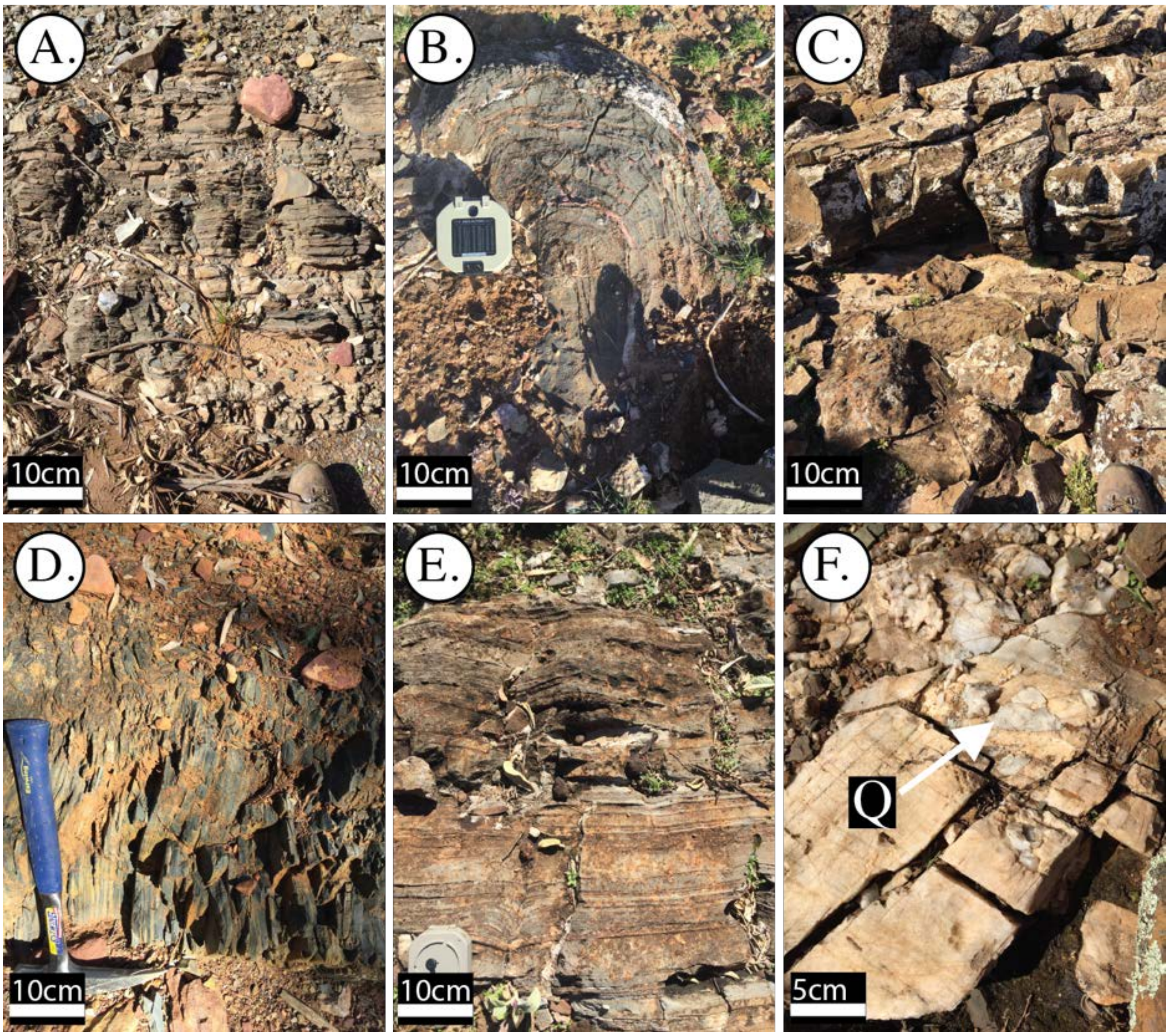

Figure 8-Example outcrop exposures for inclusion lithofacies. Outcrop photograph of A) Lithofacies 1-lime mudstone, B) Lithofacies 2-silty limestone, C) Lithofacies 3-silty limestone, D) Lithofacies 4-siltstone, E) Lithofacies 5-sandy dolomite, and F) calcite veins that cross-cut Lithofacies 4 (secondary quartz vein annotated by white arrow) located in limestone inclusion 3 (stratigraphic section 3) in Patawarta Diapir. Each photograph corresponds to the lithofacies in Fig. 10-11; Table 3-6.

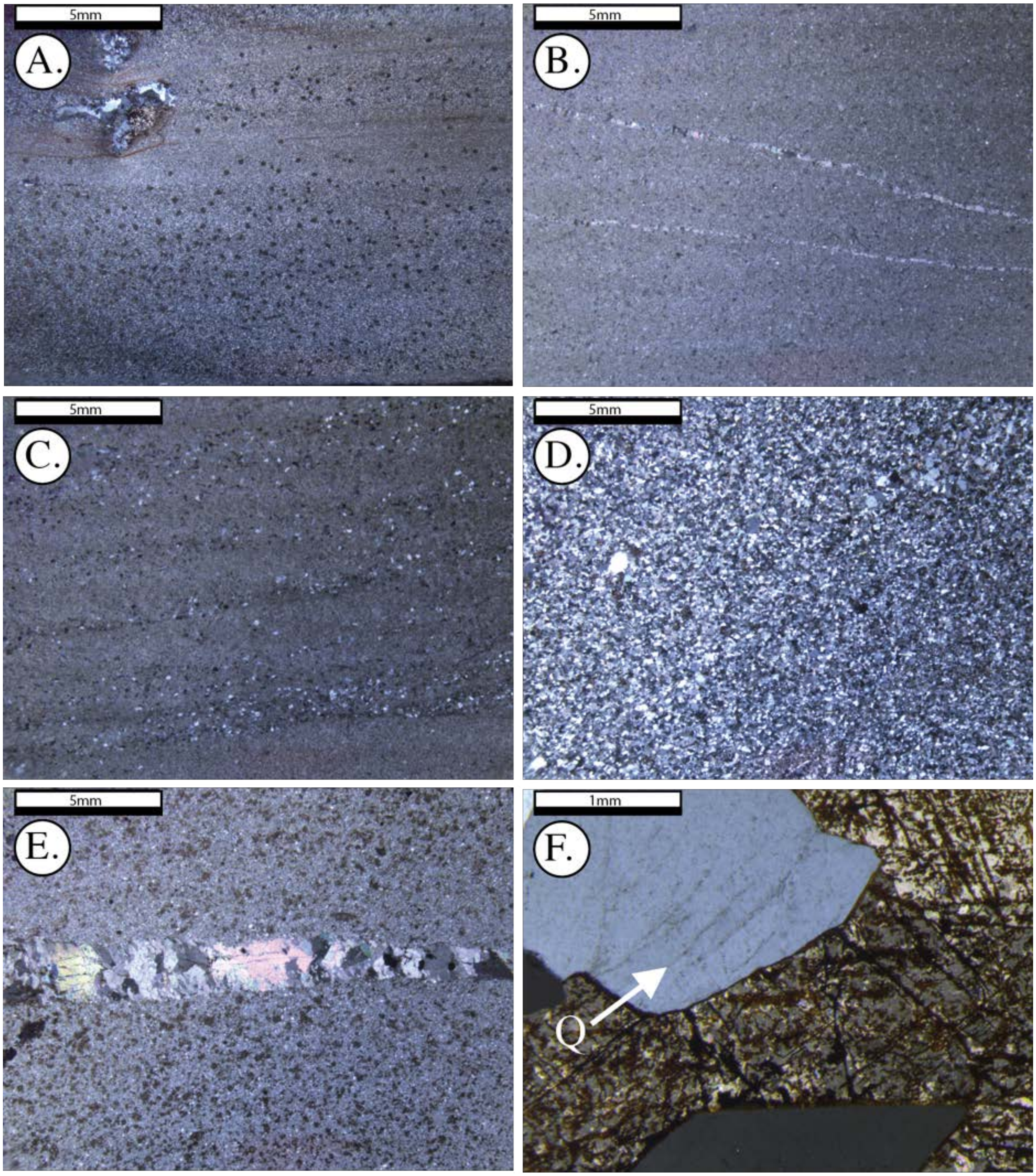

Figure 9-Photomicrographs in cross-polarized light of A) Lithofacies 1-lime mudstone, B) Lithofacies 2-silty limestone, C) Lithofacies 3-silty limestone, D) Lithofacies 4-siltstone, E) Lithofacies 5-silty dolomite, and F) calcite veins that cross-cut Lithofacies 4 (secondary quartz vein annotated by white arrow) located in inclusion 3 (stratigraphic

section 3) in Patawarta Diapir. Each photomicrograph corresponds to the lithofacies in Figs. 10-11; Table 3-6.

INCLUSION CHARACTERISTICS					
Inclusion	Length	Width	Dip	Folds	Stratigraphy
1	1.5km	0.3km	45-90	none	
2	1.0km	0.4km	20-60	recumbent	
3	0.8km	0.25km	30-75	none	
4	1.0km	0.2km	40-90	none	
5	1.1km	1.2km	30-60	recumbent	

Table 3-Size and structural characteristics and lithofacies succession of sedimentary inclusions in the Patawarta Diapir.

SUMMARY OF INTRASALT INCLUSION SEDIMENTOLOGY					
Lithofacies	Lithology	Color	Bedding	Grain Size	Sedimentary Structures
lower dolomite	sandy-silty dolomite	tan	5-10 mm	silt, medium sandstone	horizontal to wavy laminae-bedding
green siltstone	siltstone, silty limestone	dark green	1-5 cm	silt	horizontal laminae-bedding
upper limetsone	lime mudstone, silty limestone	tan	5 mm-30 cm	silt	horizontal laminae-bedding
middle limestone	lime mudstone, silty limestone	gray, tan	1 mm-10 cm	silt	horizontal laminae-bedding
lower limestone	lime mudstone, silty limestone	gray, tan	1 mm-5 cm	silt	horizontal laminae-bedding

Table 4-Summary of intrasalt inclusion sedimentology inside Patawarta Diapir.

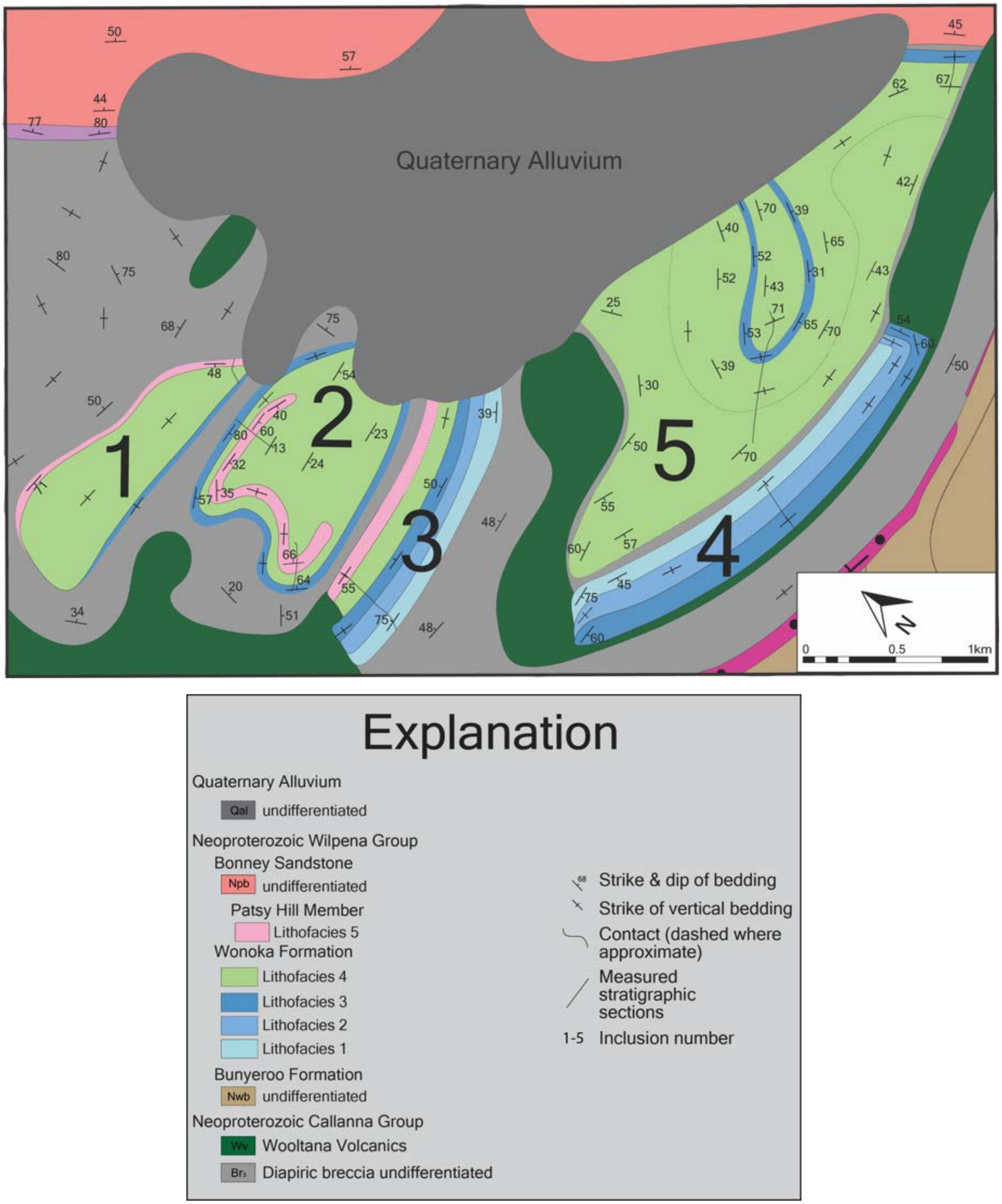

Figure 10-Detailed geologic map of limestone inclusions (1-5) in Patawarta Diapir. Map area is highlighted in Fig. 5. Attributes of lithofacies types within sedimentary inclusions are summarized in Table 4.

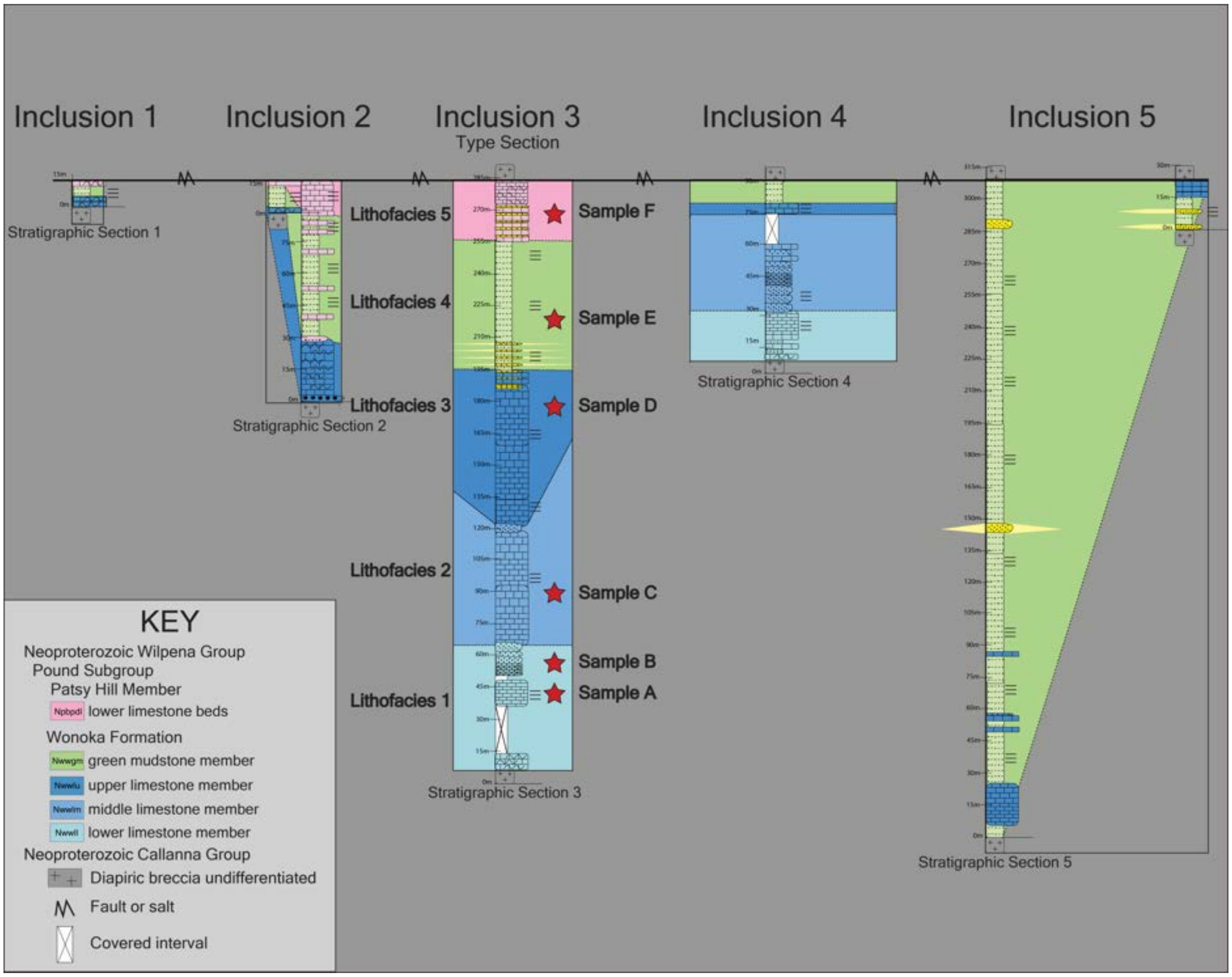

Figure 11-Detailed fence diagram of the intrasalt Ediacaran-aged Wonoka Formation and lower dolomite beds of the Patsy Hill member limestone inclusions. Locations of inclusions are shown in Fig. 10. Samples were collected from inclusion 3 in order to complete the outcrop, petrographic, and carbon isotope study.

Stratigraphy		Map Unit	SUPRASALT MINIBASIN (Gannaway, 2014)		SUBSALT MINIBASIN (Kernen et al., 2012)		INTRASALT INCLUSIONS (*this study*)				
			Thickest Section	Thinnest Section	Thickest Section	Thinnest Section	Inclusion Lithofacies	Thickest Section	Location of Thickest Section	Thinnest Section	Location of Thinnest Section
Bonney Ss		Npb	*isopachous*		40	25	*absent*				
	Patsy Hill Member	Npbpdu	105	20	55	15					
		Npbps	156	69	40	9					
		Npbpdl	43	19	40	18	5	30	3	3	1
Wonoka Formation		Nwwgm	230	97	130	7	4	200	5	6	1
		Nwwlu	246	36	80	20	3	70	3	6	1
		Nwwlm	383	30	215	20	2	55	3	30	4
		Nwwll	779	247	550	70	1	60	3	22	4
Bunyeroo Formation		Nwb	1588	32	*data not availible*		*absent*				

Table 5-Stratigraphic unit thicknesses variations of the suprasalt and subsalt minibasins that are compared to thickness trends of the intrasalt inclusions in the Patawarta Diapir (modified from Gannaway, 2014; Kernen et al., 2012). All units are in meters.

Stratigraphy			Map Unit	Depositional Environment			Depositional Sequence Stratigraphy	Halokinetic Sequence Stratigraphy		
				Intrasalt Clasts (this study)	Suprasalt Minibasin (Gannaway, 2014)	Subsalt Minibasin (Kernen et al., 2012)		Intrasalt Clasts (this study)	Suprasalt Minibasin (Gannaway, 2014)	Subsalt Minibasin (Kernen et al., 2012)
Bonney Sandstone			Npb	absent	middle shelf lower shoreface		Transgressive-Highstand Systems Tracts	absent	Minimal halokinetic deformation	Minimal halokinetic deformation
	Patsy Hill Member	unit 11	Npbpdu	absent	lagoon with washover fans & flood tidal delta	lagoon/bay	*Transgressive Surface* Lowstand Systems Tract		*CHS Boundary* Tapered CHS rim syncline	*CHS Boundary* Tapered CHS rim syncline
		unit 10	Npbps	absent	barrier island	barrier bar				
		unit 9	Npbpdl	lagoon/ lacustrine	intertidal tidal flat	main tidal channel inlet	*Sequence Boundary* Highstand Systems Tract	carapace		
Wonoka Formation		unit 8	Nwwgm	coastal plain	lagoon & subtidal to intertidal upper shoreface to foreshore	coastal plain				
		units 6-7	Nwwlu	coastal plain	foreshore upper shoreface	foreshore upper shoreface				
		unit 5	Nwwlm	coastal plain	upper shoreface lower to middle shoreface	foreshore lower to upper shoreface				
		units 1-4	Nwwll	coastal plain	lower shoreface outer shelf	lower shoreface outer shelf	*Maximum Flooding Surface*		*CHS Boundary* Tapered CHS	
Bunyeroo Formation			Nwb	absent	outer shelf or terrestrial(?)		Transgressive Systems Tract	absent		*CHS Boundary* Tapered CHS

Table 6: Compilation of the stratigraphic units surrounding Patawarta Diapir and their depositional environments, depositional, and halokinetic sequence stratigraphy for intrasalt, suprasalt, and subsalt (modified from Kernen et al., 2012; Gannaway, 2014).

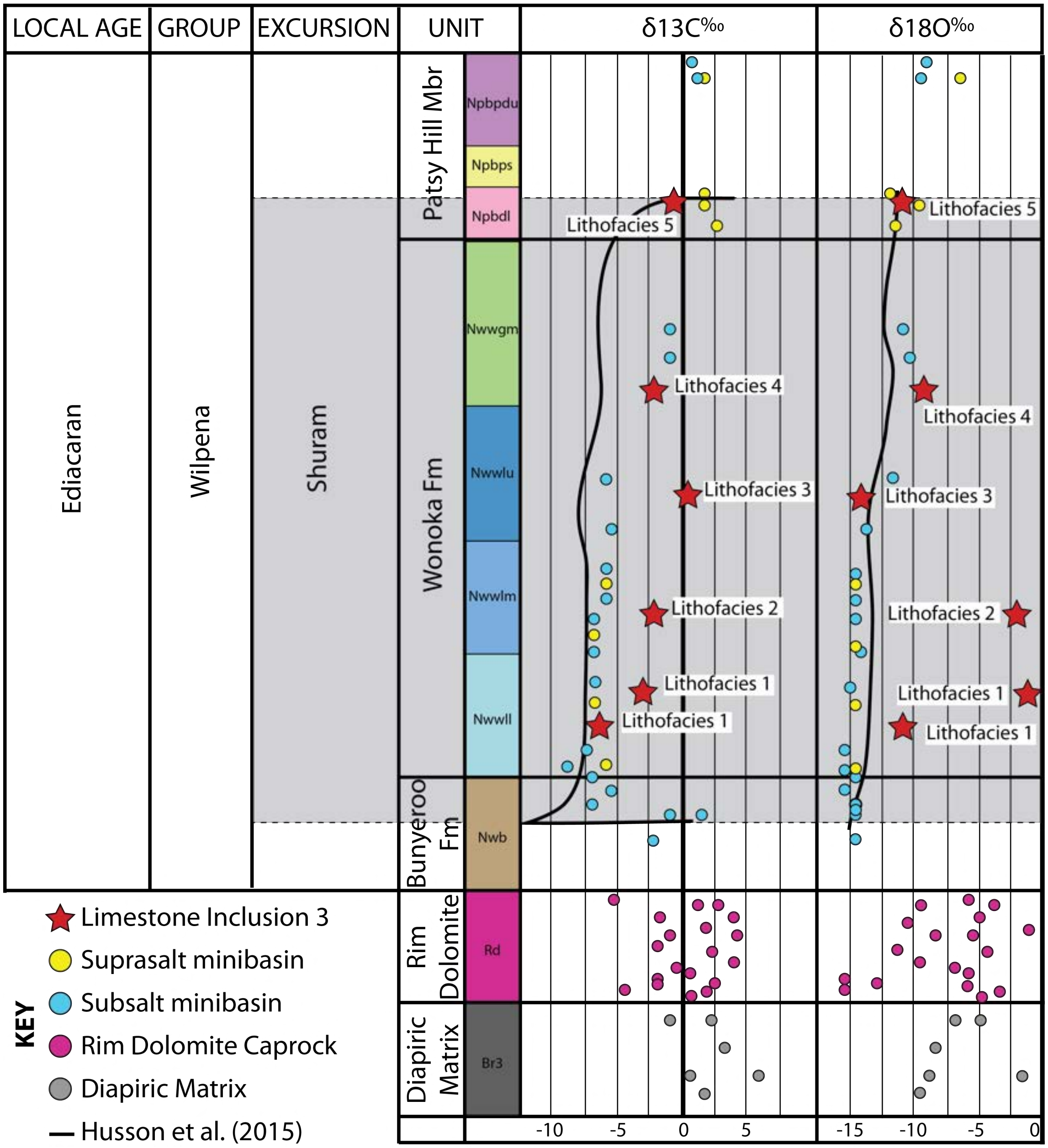

Figure 12-$\delta^{13}C$ & $\delta 18O$ isotopes used as a chemostratigraphic tool to identify Wonoka Formation and Patsy Hill member stratigraphy in the Patawarta Diapir. Stars show isotope values measured from sedimentary inclusion 3 (stratigraphic section 3) of this study. The location and stratigraphic level of the samples is shown in Figs. 10-11.

δ 18O

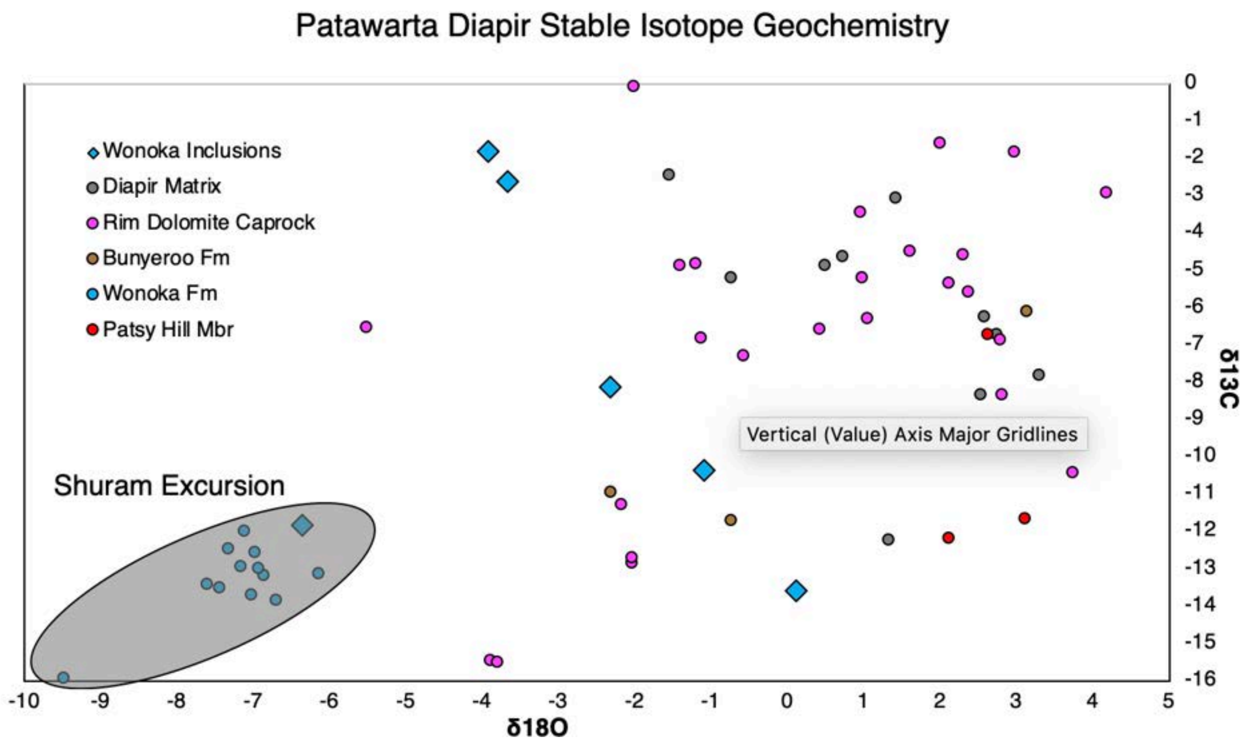

Figure 13-$\delta^{13}C$ and $\delta^{18}O$ isotopes of the Wonoka Formation inclusions located inside the Patawarta Diapir (blue diamond), diapiric matrix (grey circle), Rim Dolomite caprock (pink circle), and the Bunyeroo Formation (brown circle), Wonoka Formation (blue circle) and Patsy Hill member of the Bonney Sandstone (red circle) in the subsalt and suprasalt minbasins adjacent to Patawarta Diapir. The Shuram Excursion is highlighted by the grey oval.

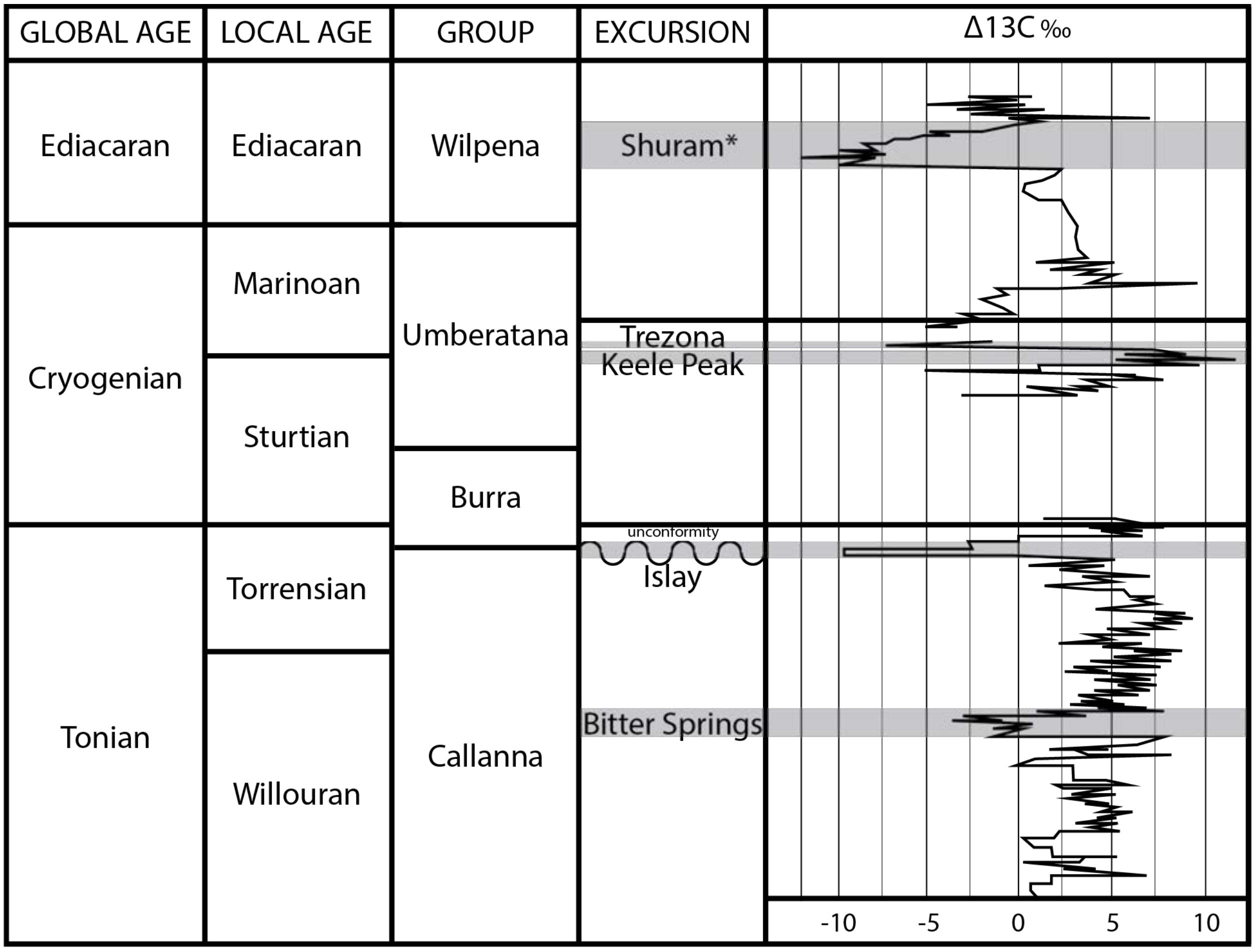

Figure 14-Global δ^{13}C isotope curve for Neoproterozoic (modified from Condon et al., 2015). Possible negative carbon isotope excursions in the Flinders Ranges inclusions could be from the Bitter Springs, Trezona, or Shuram excursions. The Islay excursion is not found in the Flinders Ranges.

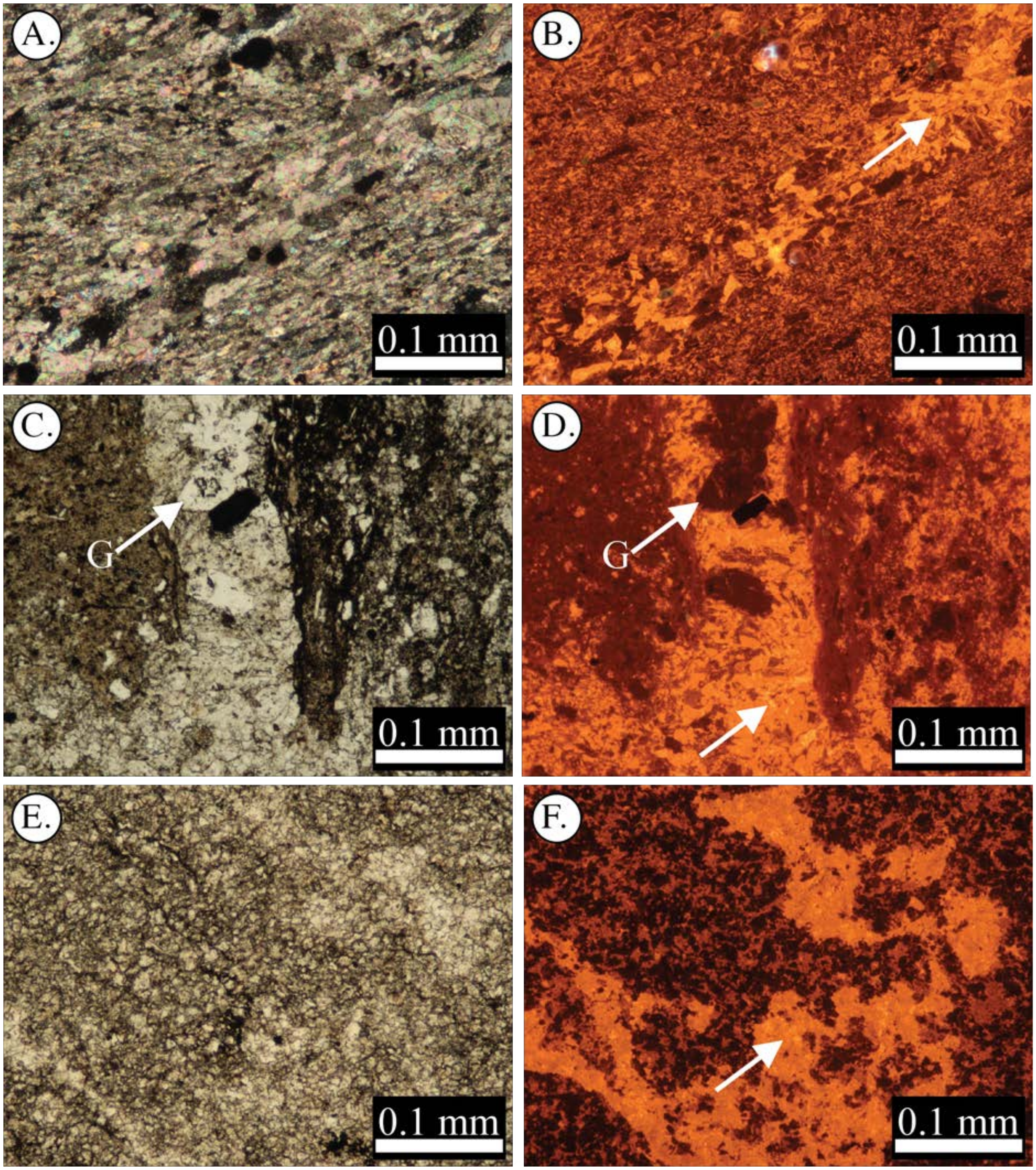

Figure 15-Photomicrographs of A) Lithofacies 1-lime mudstone in cross-polarized light, B) cathodoluminescence Lithofacies 1-lime mudstone (brown/orange fine-grained crystalline matrix) with calcite-rich (orange-yellow) veins (diagenetic alteration) cross-cutting Lithofacies 1 (white arrow), C) Lithofacies 3-silty limestone in cross-polarized light, D) cathodoluminescence Lithofacies 3-silty limestone (orange/dark orange matrix)

with calcite-rich (orange-yellow) veins (diagenetic alteration) cross-cutting Lithofacies 3 (white arrow) and quartz replacing gypsum (G), E) Lithofacies 5-silty dolomite in cross-polarized light, F) cathodoluminescence of Lithofacies 5-silty dolomite (dark brown/black) matrix with calcite-rich (orange-yellow) veins cross-cutting Lithofacies 5 (white arrow) located in inclusion 3 (stratigraphic section 3) in Patawarta Diapir. Each photomicrograph corresponds to the lithofacies in Figs. 8-11; Table 3-6.

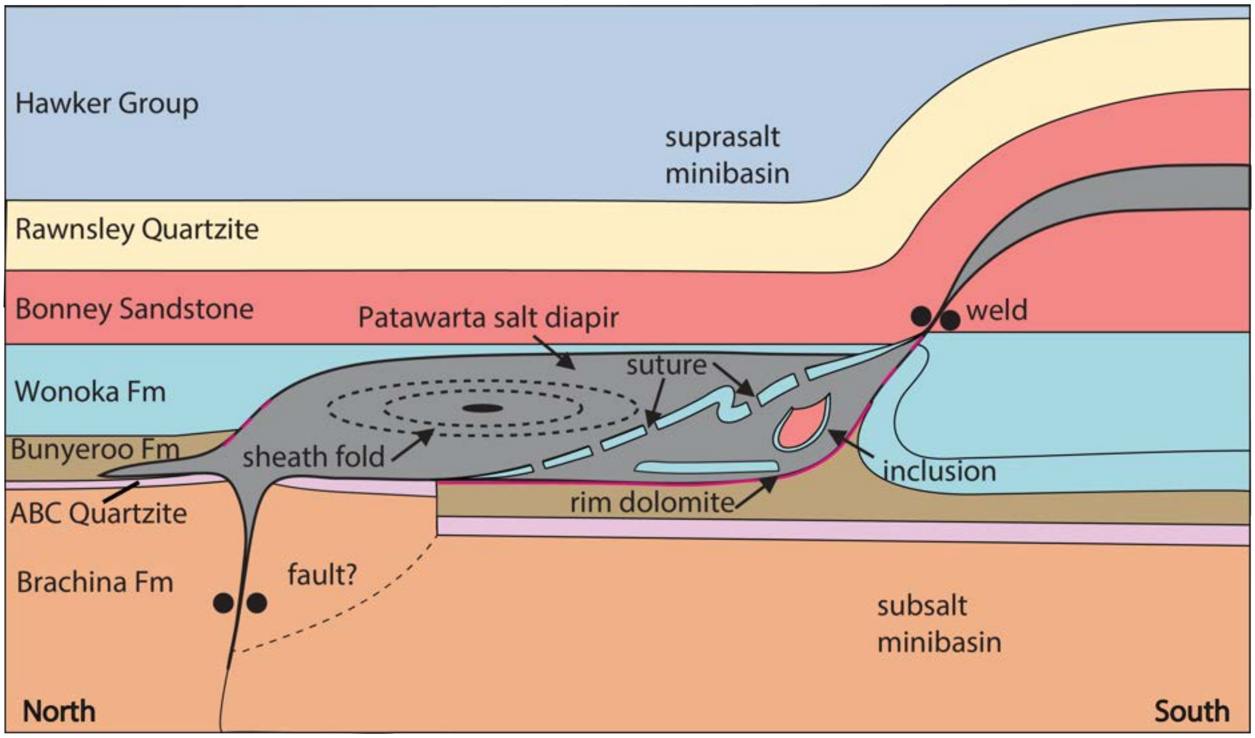

Figure 16-Schematic cross-section of the Wonoka Formation and Patsy Hill Member inclusions inside the Patawarta Diapir (modified from Hearon et al., 2015a). The LES sheath fold is located in a northern updip salt body separated by a suture (allosuture) and a second southern salt body.

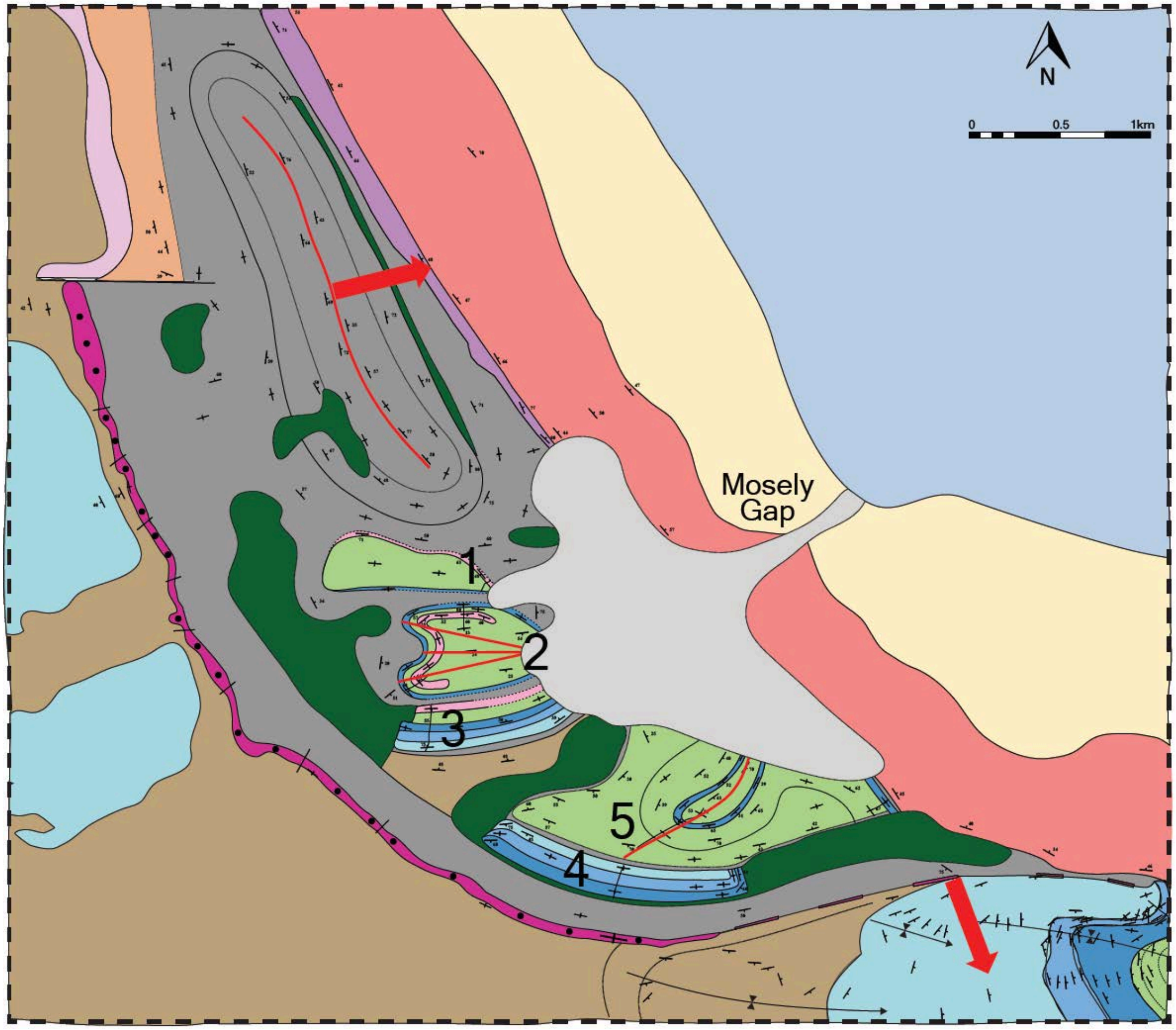

Figure 17-Geologic Map of the Patawarta Diapir, Central Flinders Ranges, South Australia (modified from Kernen et al., 2018; Rowan et al., 2019). Red lines in inclusions 2 & 5 are refolded folds, red line to the north is the axial trace of a sheath fold with the red arrow indicating the direction of salt flow (Rowan et al., 2019). The red arrow to the south is from (Hearon et al., 2015) that indicates the direction of salt flow (using the outboard halokinetic sequence fold plane to calculate direction).

Appendix

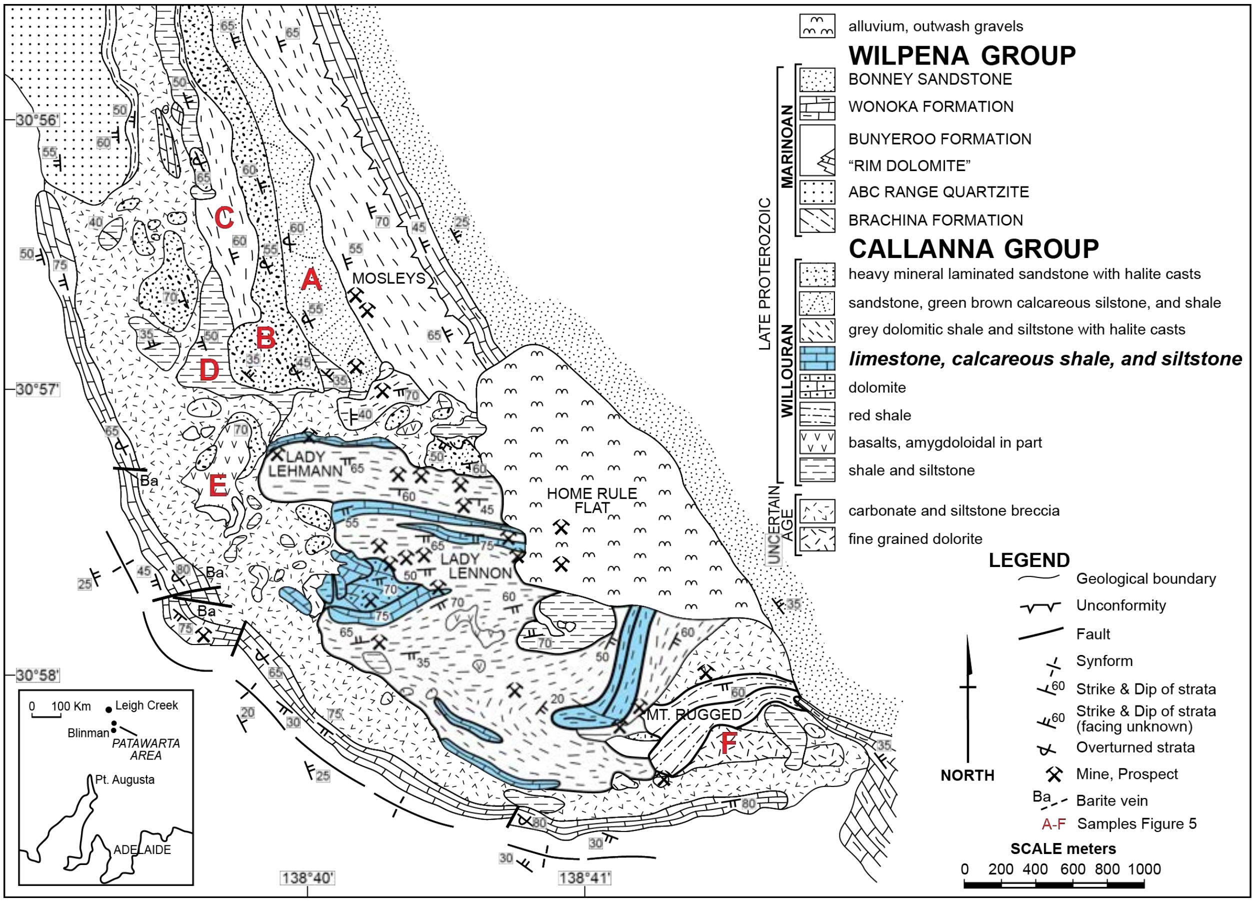

Figure 1-Geologic map of the Patawarta Diapir showing variable lithologies of inclusions in the diapiric breccia (Br_3 on Figs. 5 & 6). The anomalous limestone and calcareous siltstone and shale inclusions are highlighted in the blue (modified from Hall, 1984). Those inclusions were originally classified as Tonian-age Callanna Group stratigraphy. The results of this study suggest they are actually Ediacaran-age Wonoka Group inclusions. Outcrop photographs of A-F (red) Fig. 2 Appendix.

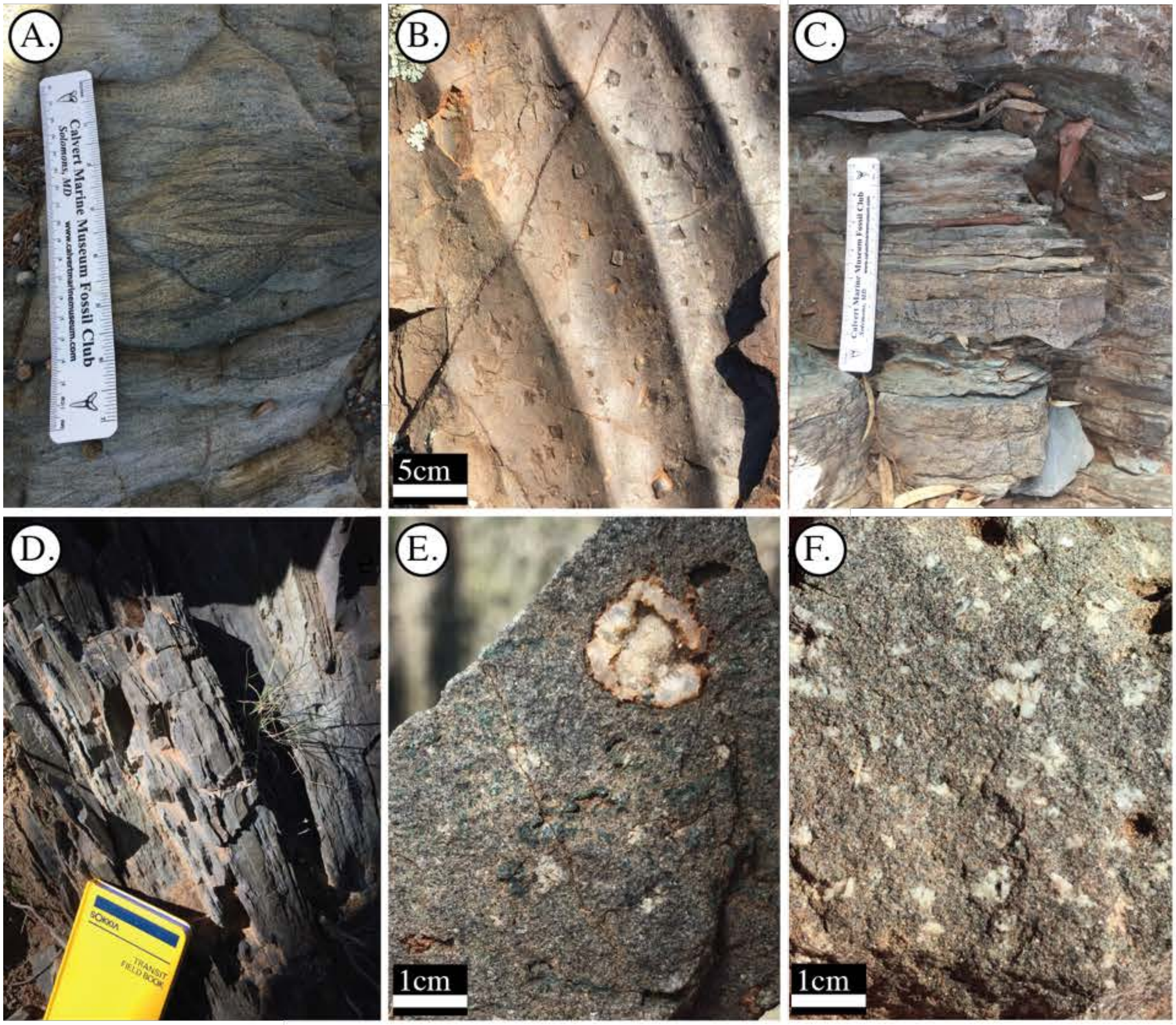

Figure 2-Outcrop photographs of Tonian-aged Callanna Group inclusions A) heavy mineral laminated sandstone and B) ripple marks and halite pseudomorphs in quartzite, C) fine interbeds of laminated heavy mineral-bearing sandstone and thinly bedded green brown calcareous siltstone and shale, D) thinly-bedded green black calcareous shale and siltstone, E) amygdaloidal basalt and F) dolerite. Location of samples annotated in Fig. 2 Appendix.